



yw

DNA 4820F-2

AD A 09 56 77

# ELECTRON INDUCED DISCHARGE MODELING, TESTING, AND ANALYSIS FOR SCATHA

12

## Volume II—Comparison of Internal Coupling Produced by Two EID Simulation Techniques

# LEVEL II

IRT Corporation  
P.O. Box 80817  
San Diego, California 92138

31 December 1978

Final Report for Period 1 September 1977—31 December 1978

CONTRACT No. DNA 001-77-C-0180

APPROVED FOR PUBLIC RELEASE;  
DISTRIBUTION UNLIMITED.

DTIC  
ELECTE  
FEB 26 1981  
S E D

THIS WORK SPONSORED BY THE DEFENSE NUCLEAR AGENCY  
UNDER RDT&E RMSS CODE X323078409 Q93QAXEE50201 H2590D.

DEC FILE COPY

Prepared for  
Director  
DEFENSE NUCLEAR AGENCY  
Washington, D. C. 20305

81 2 26 086

Destroy this report when it is no longer  
needed. Do not return to sender.

PLEASE NOTIFY THE DEFENSE NUCLEAR AGENCY,  
ATTN: STTI, WASHINGTON, D.C. 20305, IF  
YOUR ADDRESS IS INCORRECT, IF YOU WISH TO  
BE DELETED FROM THE DISTRIBUTION LIST, OR  
IF THE ADDRESSEE IS NO LONGER EMPLOYED BY  
YOUR ORGANIZATION.



UNCLASSIFIED

SECURITY CLASSIFICATION OF THIS PAGE (When Data Entered)

19 REPORT DOCUMENTATION PAGE		READ INSTRUCTIONS BEFORE COMPLETING FORM
18 1. REPORT NUMBER DNA 4820F-2	2. GOVT ACCESSION NO. AD-A095677	3. RECIPIENT'S CATALOG NUMBER 9
6 4. TITLE (and Subtitle) ELECTRON INDUCED DISCHARGE MODELING, TESTING, AND ANALYSIS FOR SCATHA. Volume II. Comparison of Internal Coupling Produced by Two EID Simulation Techniques.		5. TYPE OF REPORT & PERIOD COVERED Final Report for Period 1 Sep 77-31 Dec 78.
10 6. AUTHOR R./Keyser J. M./Wilkenfeld	14	7. PERFORMING ORG. REPORT NUMBER IRT-8161-018-1
	15	8. CONTRACT OR GRANT NUMBER(s) DNA 001-77-C-0180
9. PERFORMING ORGANIZATION NAME AND ADDRESS IRT Corporation P.O. Box 80817 San Diego, California 92138		10. PROGRAM ELEMENT, PROJECT, TASK AREA & WORK UNIT NUMBERS 16 Subtask: Q93QAXEE502-01
11. CONTROLLING OFFICE NAME AND ADDRESS Director Defense Nuclear Agency Washington, D.C. 20305	11	12. REPORT DATE 31 December 1978
14. MONITORING AGENCY NAME & ADDRESS (if different from Controlling Office) 17) E502	12) 85	13. NUMBER OF PAGES 86
		15. SECURITY CLASS (of this report) UNCLASSIFIED
		15a. DECLASSIFICATION DOWNGRADING SCHEDULE
16. DISTRIBUTION STATEMENT (of this Report)  Approved for public release; distribution unlimited.		
17. DISTRIBUTION STATEMENT (of the abstract entered in Block 20, if different from Report)		
18. SUPPLEMENTARY NOTES  This work sponsored by the Defense Nuclear Agency under RDT&E RMSS Code X323078409 Q93QAXEE50201 H2590D.		
19. KEY WORDS (Continue on reverse side if necessary and identify by block number) Electrical Testing Spacecraft Charging Electron Induced Discharge Effects Electron Induced Discharge Simulation SCATHA		
20. ABSTRACT (Continue on reverse side if necessary and identify by block number) A combined analytical and experimental program has been carried out to understand, simulate, and model the effects produced by the coupling of space electron induced electrostatic discharges (EID) into satellite structures. The program had five main tasks: to develop a worst case model for EID defined as a current source and to incorporate it into an SGEMP code for coupling analyses; to construct and electrically test a scale model (SCATSAT) of the P78-2 (SCATHA) spacecraft; to make a comparison between test results and model → next page		

DD FORM 1 JAN 73 1473 EDITION OF 1 NOV 65 IS OBSOLETE

UNCLASSIFIED

SECURITY CLASSIFICATION OF THIS PAGE (When Data Entered)

409388 76

UNCLASSIFIED

SECURITY CLASSIFICATION OF THIS PAGE(When Data Entered)

20. ABSTRACT (Continued)

cont → prediction; and to specify a strawman set of electrical test procedures for simulating the response of spacecraft to ESD for incorporation into a Spacecraft Charging Military Standard; to compare the internal response of the SCATSAT to two techniques simulating different aspects of the discharge, the arc itself and the blowoff electrons. The work carried out under the first four tasks is discussed in Volume I of this report.)

↳ A high fidelity physical electromagnetic model of the SCATHA P78-2 space vehicle has been tested for internal responses to two techniques simulating different aspects of an electrostatic discharge, the arc itself and blowoff of charged particles. The responses measured on the model were compared to responses measured on the P78-2 for a Mil-Std 1541 arc injection to test the model's fidelity, with reasonable agreement resulting. The model responses show that simulation of charge blowoff produces larger internal responses per ampere of drive than does a simple arc simulation, except when the arc is coupled directly to the measurement point. Measured responses for the two techniques spanned a range of four orders of magnitude from 0.01 to 100 mV/ampere. Special implications of simulating discharges on a real solar array were discovered and are discussed. Construction of the model, the drive techniques, and the instrumentation are presented in detail.

UNCLASSIFIED

SECURITY CLASSIFICATION OF THIS PAGE(When Data Entered)

## PREFACE

Many people contributed to the success of this effort and we wish to acknowledge and thank them for their individual efforts. At IRT, the test object modifications were accomplished by Mr. Grant Snellon and Mr. Andy Weiman. Mr. Weiman also contributed significantly to troubleshooting the experiment, building the arc pulser, and nurturing the fiber optic data links.

At MMC, Denver, Mr. Bob Lewis, Mr. Ken Richardson, Mr. Bob Loveland, and many others provided data on the P78-2 configuration, the EMC tests, and the arc pulser which were most helpful.

At Aerospace, Mr. Al Vampola, Mr. Dom Scrooc, Dr. Roy Lewis, and Mr. Jim Coge were most helpful in answering our questions and in supplying P78-2 test data.

Major Carl Bloemker of Defense Nuclear Agency and Captain M. H. Bunn, Major George Kuck, and Lt. Colonel John Durrett of SAMSO all were instrumental in bringing together the participants and creating a spirit of cooperation.

Finally, thanks to Mr. Wallace Danielson and his staff, particularly Ms. Yvonne Hearn and Mr. Bill Quintero, for producing this attractive final report, and to Ms. Betty Hill for typing the draft.

<b>Accession For</b>	
NTIS GRA&I	<input checked="" type="checkbox"/>
DTIC TAB	<input type="checkbox"/>
Unannounced Justification	<input type="checkbox"/>
By _____	
Distribution/	
<b>Availability Codes</b>	
Dist	Avail and/or Special
<b>A</b>	

CONVERSION FACTORS FOR U.S. CUSTOMARY TO  
METRIC (SI) UNITS OF MEASUREMENT

TO CONVERT FROM	TO	MULTIPLY BY
angstrom	meters (m)	1.000 000 X E -10
atmosphere (normal)	kilo pascal (kPa)	1.013 25 X E +2
bar	kilo pascal (kPa)	1.000 000 X E +2
bar	meter <sup>2</sup> (m <sup>2</sup> )	1.000 000 X E -28
British thermal unit (thermochemical)	joule (J)	1.054 350 X E +3
calorie (thermochemical)	joule (J)	4.184 000
cal (thermochemical)/cm <sup>2</sup>	mega joule/m <sup>2</sup> (MJ/m <sup>2</sup> )	4.184 000 X E -2
curie	giga becquerel (GBq) <sup>a</sup>	3.700 000 X E +1
degree (angle)	radian (rad)	1.745 329 X E -2
degree Fahrenheit	degree kelvin (K)	$T_K = (t^{\circ}F + 459.67)/1.8$
electron volt	joule (J)	1.602 19 X E -19
erg	joule (J)	1.000 000 X E -7
erg/second	watt (W)	1.000 000 X E -7
foot	meter (m)	3.048 000 X E -1
foot-pound-force	joule (J)	1.355 818
gallon (U.S. liquid)	meter <sup>3</sup> (m <sup>3</sup> )	3.785 412 X E -3
inch	meter (m)	2.540 000 X E -2
jerk	joule (J)	1.000 000 X E +9
joule/kilogram (J/kg) (radiation dose absorbed)	Gray (Gy) <sup>**</sup>	1.000 000
kilotons	terajoules	4.183
kip (1000 lbf)	newton (N)	4.448 222 X E +3
kip/inch <sup>2</sup> (ksi)	kilo pascal (kPa)	6.894 757 X E +3
ktap	newton-second/m <sup>2</sup> (N-s/m <sup>2</sup> )	1.000 000 X E +2
micron	meter (m)	1.000 000 X E -6
mil	meter (m)	2.540 000 X E -5
mile (international)	meter (m)	1.609 344 X E +3
ounce	kilogram (kg)	2.834 952 X E -2
pound-force (lbf avoirdupois)	newton (N)	4.448 222
pound-force inch	newton-meter (N·m)	1.129 848 X E -1
pound-force/inch	newton/meter (N/m)	1.751 268 X E +2
pound-force/foot <sup>2</sup>	kilo pascal (kPa)	4.788 026 X E -2
pound-force/inch <sup>2</sup> (psi)	kilo pascal (kPa)	6.894 757
pound-mass (lbm avoirdupois)	kilogram (kg)	4.535 924 X E -1
pound-mass-foot <sup>2</sup> (moment of inertia)	kilogram-meter <sup>2</sup> (kg·m <sup>2</sup> )	4.214 011 X E -2
pound-mass/foot <sup>3</sup>	kilogram/meter <sup>3</sup> (kg/m <sup>3</sup> )	1.601 846 X E +1
rad (radiation dose absorbed)	Gray (Gy) <sup>**</sup>	1.000 000 X E -2
roentgen	coulomb/kilogram (C/kg)	2.579 760 X E -4
shake	second (s)	1.000 000 X E -8
slug	kilogram (kg)	1.459 390 X E +1
torr (mm Hg, 0° C)	kilo pascal (kPa)	1.333 22 X E -1

<sup>a</sup> The becquerel (Bq) is the SI unit of radioactivity; 1 Bq = 1 event/s.

<sup>\*\*</sup> The Gray (Gy) is the SI unit of absorbed radiation.

## TABLE OF CONTENTS

PREFACE . . . . .	1
CONVERSION TABLE . . . . .	2
LIST OF ILLUSTRATIONS . . . . .	3
LIST OF TABLES . . . . .	5
EXECUTIVE SUMMARY . . . . .	7
1. INTRODUCTION . . . . .	9
2. EXPERIMENT DESCRIPTION. . . . .	13
General Setup and Instrumentation . . . . .	13
SCATSAT Test Object . . . . .	17
Injection Points and Methods . . . . .	22
Arc Injection . . . . .	25
Injector Connections . . . . .	26
Data Taking . . . . .	27
3. RESULTS . . . . .	31
P78-2 Results . . . . .	31
SCATSAT Results . . . . .	33
Comparisons . . . . .	59
Calculation Results . . . . .	69
4. SOLAR ARRAY EXCITATION . . . . .	73
5. CONCLUSIONS AND RECOMMENDATIONS . . . . .	75
REFERENCES . . . . .	79

### List of Illustrations

Figure	Page
1 Arc injection points on the P78-2 and on SCATSAT . . . . .	10
2 TPM and SC1-8B measurements on P78-2 which were simulated on the SCATSAT . . . . .	11
3 General layout of experimental area . . . . .	14
4 Photo of SCATSAT in test area . . . . .	15
5 Isolated instrumentation configuration schematic . . . . .	16
6 Boom modifications . . . . .	18
7 Aft omni antenna configuration . . . . .	19
8 SC7-3 experiment configuration. . . . .	19
9 High and low Z TPM antenna configuration details. . . . .	20

## List of Illustrations

Figure		Page
10	Top view of box 3B/4B detail . . . . .	20
11	Internal views of SCATSAT. . . . .	21
12	Patch panel and approximate cable routing . . . . .	23
13	Examples of two injection techniques to arc point 8 . . . . .	24
14	Capacitive direct injection waveforms . . . . .	24
15	Arc pulser schematic diagram . . . . .	25
16	Sample arc current waveform. . . . .	27
17	CDI current waveform at point 4 only . . . . .	29
18	CDI response waveforms for injection at point 9 on solar array . . . . .	34
19	Arc injection response waveforms for injection at point 9 to the solar array substrate . . . . .	35
20	CDI response waveforms for injection at point 2 on central structure. . . . .	36
21	Arc injection response waveforms for injection at point 2 on central structure . . . . .	37
22	CDI response waveforms for injection at point 11 on aft end . . . . .	38
23	Arc injection response waveforms for injection at point 11 on aft end . . . . .	39
24	CDI response waveforms for injection at point 4 on end of SC11-1 boom . . . . .	40
25	Arc injection response waveforms for injection at point 4 on end of SC11-1 boom . . . . .	41
26	Detail of injection point 9 . . . . .	42
27	Isolated CDI response waveforms for injection at point 4 . . . . .	43
28	Comparison of arc and capacitive responses at drive point 1 for a one ampere drive current . . . . .	48
29	Comparison of arc and capacitive responses at drive point 2 for a one ampere drive current . . . . .	49
30	Comparison of arc and capacitive responses at drive point 7 for a one ampere drive current . . . . .	50
31	Comparison of arc and capacitive responses at drive point 3 for a one ampere drive current . . . . .	51
32	Comparison of arc and capacitive responses at drive point 8 for a one ampere drive current . . . . .	52
33	Comparison of arc and capacitive responses at drive point 9 for a one ampere drive current . . . . .	53
34	Comparison of arc and capacitive responses at drive point 5 for a one ampere drive current . . . . .	54

### List of Illustrations

Figure		Page
35	Comparison of arc and capacitive responses at drive point 6 for a one ampere drive current . . . . .	55
36	Comparison of arc and capacitive responses at drive point 10 for a one ampere drive current . . . . .	56
37	Comparison of arc and capacitive responses at drive point 11 for a one ampere drive current . . . . .	57
38	Comparison of arc and capacitive responses at drive point 4 for a one ampere drive current . . . . .	58
39	Arc current . . . . .	60
40	CDI current . . . . .	60
41	Fast Fourier Transform of arc current . . . . .	61
42	Fast Fourier Transform of CDI current. . . . .	61
43	Peak signal observed on "PCU Ground" for capacitive direct injection at the eleven drive points. . . . .	65
44	Peak signal observed on "Upper Array" for capacitive direct injection at the eleven drive points. . . . .	66
45	Peak signal observed on "PCU Ground" for arc injection at the eleven drive points . . . . .	67
46	Peak signal observed on "PCU Ground" for arc injection at the eleven drive points . . . . .	68
47	Schematic of real solar array with EID injection. . . . .	74

### List of Tables

Table		Page
1	P78-2 and SCATSAT Measurements . . . . .	9
2	Arc Characteristics vs Gap Width . . . . .	26
3	Pulser Attachment Points . . . . .	27
4	Results of FODL Calibration . . . . .	28
5	P78-2 Response Data . . . . .	32
6	P78-2 SC1-8B Cable Responses . . . . .	32
7	Frequencies in MHz Observed in SCATSAT Measurements . . . . .	45
8	Comparison of High to Mid Frequency Content for CDI and Arc Currents .	62
9	Estimated P78-2 Critical Circuit Responses . . . . .	71

*Blank*

## EXECUTIVE SUMMARY

Electrical responses of the SCATSAT, a physical electromagnetic model of the SCATHA P78-2 space vehicle, were measured for two drive techniques simulating different aspects of an electron induced discharge (EID). One, arc injection, simulates a punchthrough discharge while the second, capacitive direct injection, simulates the blowoff of charged particles which is the principal consequence of the discharge. The injection locations and measurement points on the SCATSAT corresponded to those used in arc injections to the real P78-2 space vehicle. Comparisons between the SCATSAT and P78-2 responses were made to test the validity of the electromagnetic model and to estimate the response of the P78-2 to a CDI simulation of charge blowoff.

Past analyses and tests have shown that blowoff charge and its CDI simulation cause larger external responses on a simple object per ampere of drive than does arc injection. A major purpose of this program was to determine if the same is true for internal (cable) coupling in an object of satellite like complexity, for it is these responses which are of real interest for satellite EID survivability. The results are also useful to aid in understanding responses of the P78-2 once it is on orbit and in developing an adequate military standard test for EID effects.

The measured SCATSAT CDI responses per ampere of drive current were larger than the arc responses in every case except those few where the injection point was directly coupled to the measurement point, i.e., those associated with the solar array. Then arc injection produced larger responses. Response comparisons show that the SCATSAT is a good but not perfect simulation of the P78-2, the principal difference being a higher degree of shielding (lower transfer function) in the SCATSAT than in the P78-2, probably because not all penetrations have been included in the model. Calculations based on the measured responses show that the most sensitive P78-2 critical circuit threshold would not have been exceeded during the space vehicle arc injections but that threat level CDI, or arc injections a factor of two to five higher, would have caused the threshold to be exceeded. The first calculation is supported by the MMC EMC tests which reported "no anomalies as a result of the static discharge to the vehicle." The comparisons also indicated a possible problem in EID simulation

quality for arcs on a real solar array resulting from the polarity and illumination sensitive conductivity of real cells. However, these calculations need further validation through a better definition of the P78-2 transfer function.

We conclude from the tests and calculations the following:

1. The P78-2 is likely to experience upsets once it is on orbit
2. That threat level CDI simulation of charge blowoff should be added to the present MIL-1541 arc discharge tests with emphasis on proper injection polarity for EID qualification
3. That the effects of solar array illumination on EID simulation quality should be studied along with the continuing simulation validation efforts.

Because of finding (1), and to relate the observed discharge response measurements to the discharge stimulus, it is important to develop a transfer function model for the P78-2 based on a coupling and susceptibility analysis and model testing to interpret the on orbit behavior of the P78-2.

The result of the simulation testing should be paralleled by a continuation of the analytical effort in which a parametric sensitivity study is carried out to determine how each element of the threat: amplitude, frequency content, and method of coupling, affects the response. Such activity was begun in Phase I of this program and should be completed. An evaluation should also be made of which aspects of the response produced are most critical in producing EID induced upset or damage as a guide to response simulation.

## 1. INTRODUCTION

A second phase of testing on the SCATSAT electromagnetic model of the P78-2 spacecraft has been completed and is reported here. The objective of this experimental effort was to obtain data on the internal coupling produced by two types of electrical excitation at specific drive points on the SCATSAT model. The excitations are applied to eleven different points as listed and diagrammed in Figure 1. Five of the measurement points are listed in Table 1 and diagrammed in Figure 2. These are the excitation and measurement points used in the Martin Marietta Corporation (MMC) arc injection tests of the P78-2 spacecraft (Refs. 1,2)

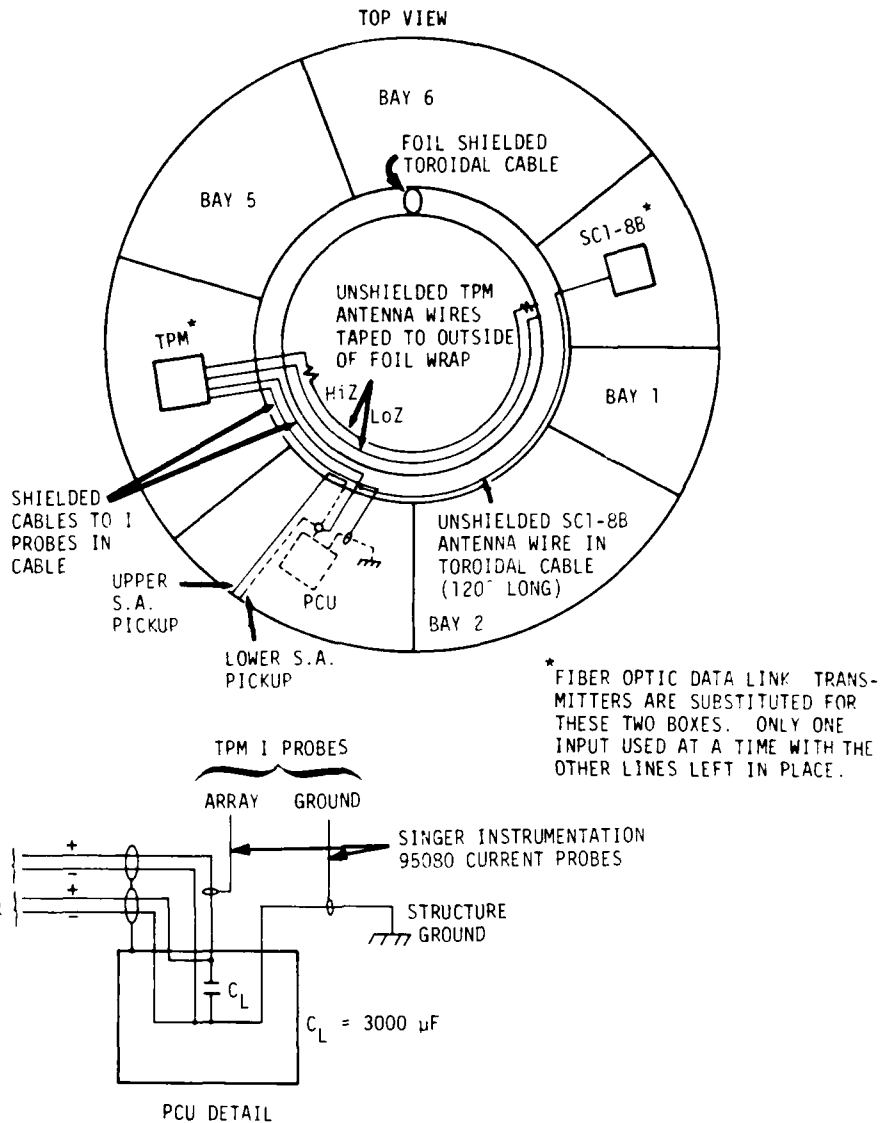
**Table 1. P78-2 and SCATSAT Measurements**

P78-2 Experiment	Measurement Name	Description
TPM*	High Z	Unshielded half loop of wire taped to outside of toroidal cable bundle shield. Far end terminated with 100 K $\Omega$ , TPM end has 10K series resistor into 50 $\Omega$ load.
TPM	Low Z	Same as high Z except far end is grounded and no series resistance.
TPM	Upper Array	A current probe on the + wire of the upper solar array.
TPM	PCU Ground	A current probe on the wire connecting the PCU to the spacecraft single point ground.
SC1-8B	Cable	A 120 <sup>o</sup> length of unshielded wire in the toroidal bundle, under the overall shield.

\* Transient Pulse Monitor

The excitation methods consisted of an arc injection similar to that used by MMC and a capacitive direct injection (CDI). The first excitation simulates one aspect of the electron induced discharge (EID), a punchthrough breakdown. The second excitation simulates a second and possibly more important aspect (from the standpoint of amplitude of satellite structural response), the emission of charged particles from the surface of the satellite in a blowoff discharge. A previous analysis and test program (Ref. 3) has demonstrated the relative excitation of a simple object, a right circular





RT-17142

**Figure 2. TPM and SC1-8B measurements on P78-2 which were simulated on the SCATSAT**

The MMC arc test on the P78-2 also monitored, indirectly, the signals on spacecraft wiring by looking for anomalies in spacecraft operation as the injections occurred. If no anomalies were detected, then the coupled signals were presumably below circuit thresholds, which were specified in the P78-2 test plan for twelve identified critical circuits. That is, there is a positive safety margin of unknown value.

However, if the on orbit electron induced discharge results in blowoff which causes significantly greater coupling than the arc injection, then these margins may go negative and the upset thresholds would be exceeded. To help determine these margins, tests were run using a CDI simulation of blowoff. The SCATSAT model contains actual spacecraft cables representative of the routings of the most sensitive and least sensitive P78-2 critical circuits. Since the SCATSAT has no electronics simulation to monitor for anomalies, the actual load voltage on these two lines were measured for comparison to the critical circuit threshold voltages given in Ref. 2. Thus, the test matrix consists of seven measurements for injection at eleven points using two techniques. These data and the published P78-2 arc data (Ref. 4,5) form the basis for making predictions of P78-2 performance for CDI simulation of blowoff discharge.

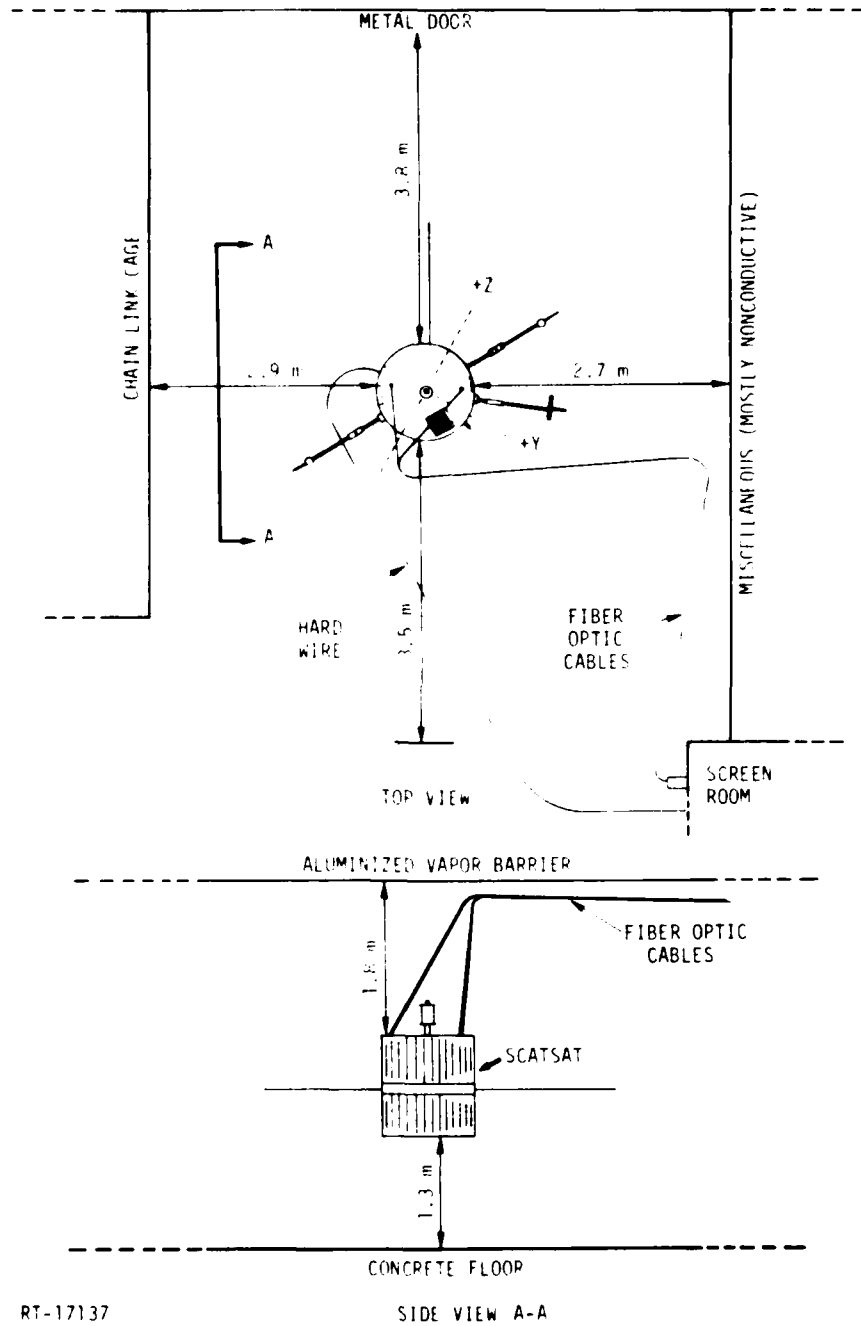
## 2. EXPERIMENT DESCRIPTION

The planned experimental effort was described in the Draft Test Plan (Ref. 6) of September 29, 1978. The actual test adhered quite faithfully to the test plan except that all of the CDI testing was done first and the arc testing later. This was because of difficulty encountered in building a satisfactory arc pulser. The duration of the test effort was extended to five weeks because of this difficulty and to do five additional arc injections which are discussed later. The key features of the experiment are described here.

### GENERAL SETUP AND INSTRUMENTATION

The general physical layout of the test area is shown in Figure 3, with the SCATSAT booms partially extended and oriented as shown. A photograph of the SCATSAT appears in Figure 4 which shows the boom configuration more clearly. The fiber optic cables were suspended overhead and routed as shown. The hardwire instrumentation cable, when used, was routed straight down from the exit point near SC11-1 boom and then run on the floor to the screen room. The test stand was non-metallic as were the struts used to hold the booms in their partially deployed position. Thus the object was electromagnetically isolated except when the hardwire was used.

The isolated instrumentation configuration is shown in Figure 5. The fiber optic data links are the 400 MHz HDL links. Two of these were used though only one is shown. The data was fed into the single ended input of the transmitters and transmitted out of the satellite on the fibers. The data out of the fiber optic receivers were displayed on an oscilloscope and recorded on Polaroid film. The scope was externally triggered as shown. This is a straightforward connection for the Anvil 160 pulser used for the capacitive direct injection and as the trigger source for the arc pulser. Only a delay is required between the trigger generator and scope to offset the delay in the data link, and/or the delay between arrival of the trigger pulse and actual arc occurrence. For the CDI part of the experiment the delay was provided by long cables while a Data pulse 101 pulse generator was used to provide the longer delay required during the arc tests.



RT-17137

Figure 3. General layout of experimental area

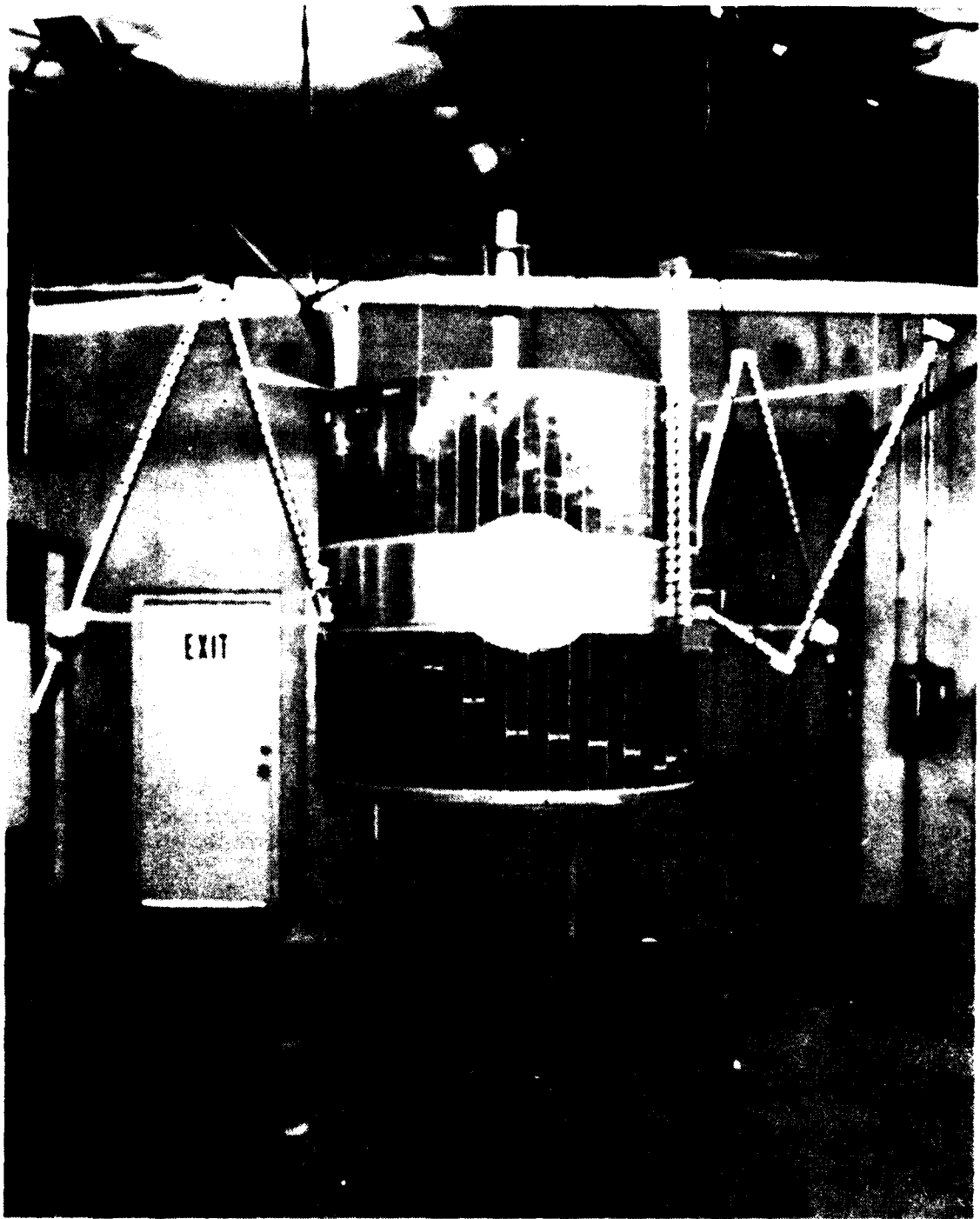
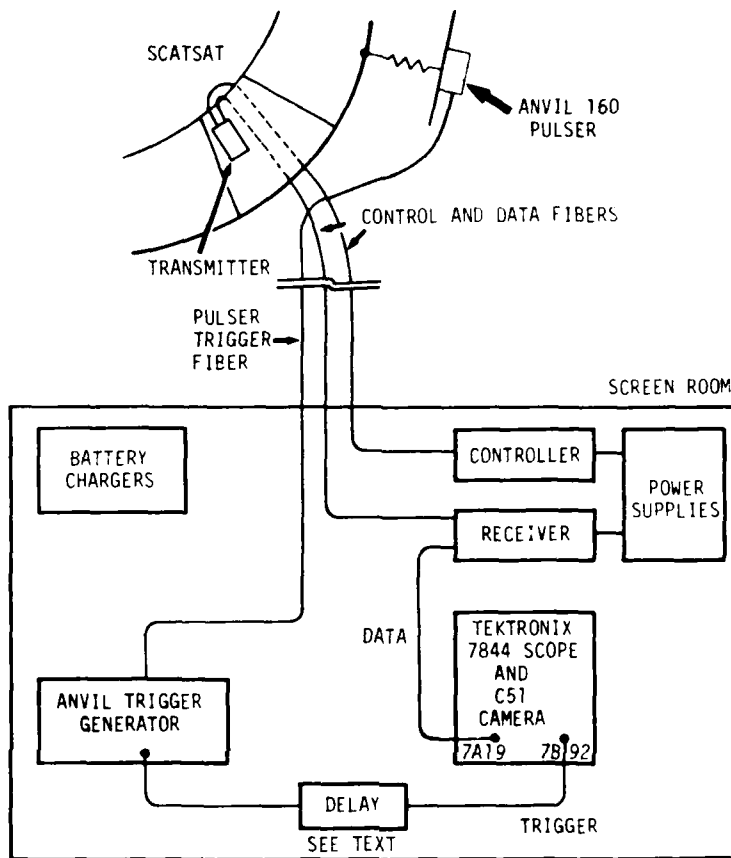


Figure 4. Photo of SCATSAT in test area



RT-17140

**Figure 5. Isolated instrumentation configuration schematic. Shown configured for a capacitive direct injection excitation. For arc injection, the plate and damping resistor were replaced with the arc pulser (see Figure 13A).**

The hardwire instrumentation configuration was similar except that the measurement point was fed directly from the patch panel on the side of SCATSAT into a 30 foot long 0.141 inch semirigid coax, through the screen room wall, and into the scope or a wideband amplifier. The amplifier was used as required because of the small amplitude (less than a millivolt) of some of the signals, for the drive levels used, and the limited sensitivity of the 7A19 scope vertical plug-in, 10 mV/div. The amplifier has a fixed gain of 20 which increases the scope sensitivity to 0.5 mV/div.

The bandwidth of the Hewlett Packard 8447D amplifier is 0.1 to 1300 MHz, the bandwidth of the 7844 oscilloscope and 7A19 plug-in is dc to 400 MHz, and the bandwidth of the fiber optic data link is 100 Hz to 400 MHz. The bandwidth of the Singer current probes is 100 KHz to 200 MHz. All are standard 50 ohm impedance.

Each HDL fiber optic data link consists of a battery powered single channel transmitter unit ~3.5 x 3.5 x 10 inches, a pair of 200 foot long fiber cables, a receiver, and a controller. Separate power supplies are required to power the receiver/controller and for charging the transmitter batteries. The transmitter is in a quiescent state to minimize battery drain until activated by an "on" command from the controller. The same "on" command also sets a digital attenuator, with individually controllable 3, 6, 12, and 24 dB steps at the transmitter input, to the positions selected by switches on the controller. This allows the input signal to the transmitter to be attenuated by any amount between 0 and 45 dB, in 3 dB steps, by remote control. The purpose of this is to keep the signal within the linear range of the link while maximizing signal to noise ratio. Verification of receipt of the selected attenuation setting by the transmitter is provided by a feedback loop activated whenever the link internal calibrator is turned on. The calibrator also allows a gain check on the link and an indication of battery condition.

When operated just within their linear range, 10 mV p-p input for one link and 5 mV p-p for the other, the practical signal to noise ratio was about 10 to 1 for the links used in this experiment.

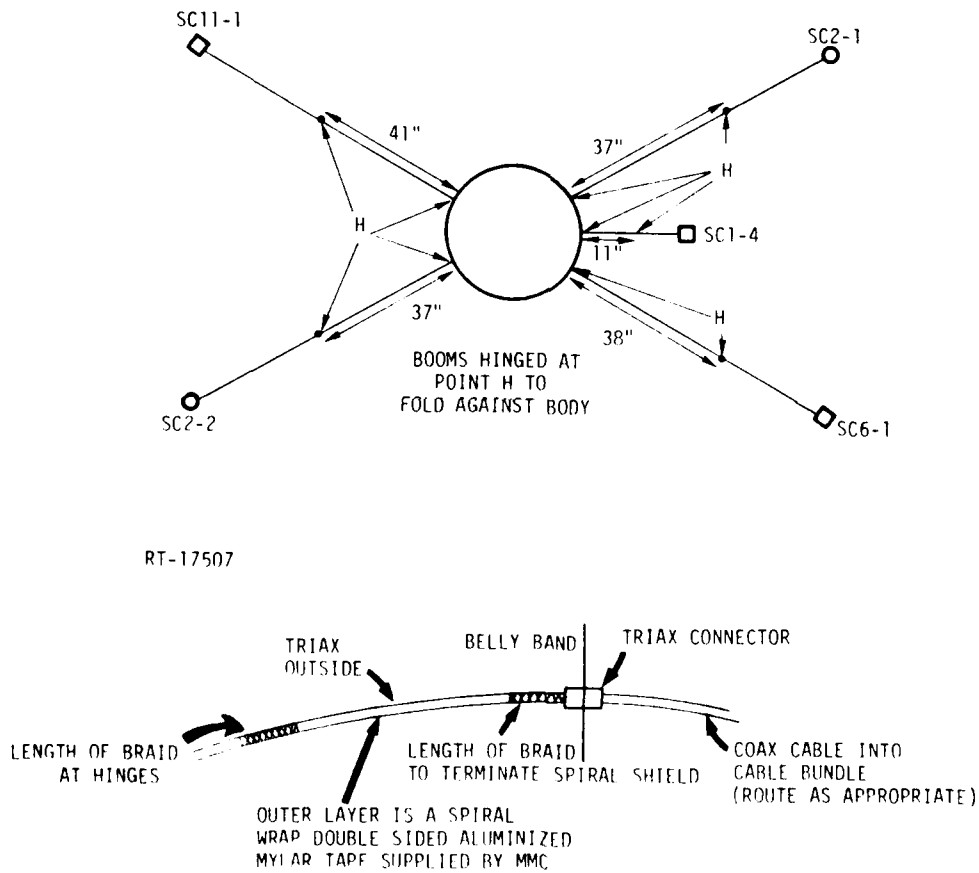
#### **SCATSAT TEST OBJECT**

The SCATSAT model of the P78-2 spacecraft is described in detail in Reference 7. That configuration did not completely meet the requirements of the present effort in that some penetrations and sensor wires were not adequately simulated. Modifications were made to incorporate the following penetrations and sensors:

1. The four boom penetrations shown in Figure 6.
2. The aft omni antenna shown in Figure 7.
3. The SC7-3 experiment shown in Figure 8.
4. The high and low Z TPM antennas as shown in Figure 9.
5. The SC1-8B "Cable" antenna shown in Figure 2.
6. Load voltage monitors for simulated critical circuits in boxes 3B and 4B as shown in Figure 10.
7. Corrected array and PCU ground current monitors and the PCU load capacitance as shown in Figure 2.

8. A five layer aluminized mylar thermal blanket on the SC11-1 experiment at the end of the boom.

Hinges had to be added to the booms as shown in Figure 6 so that they could be partially deployed per the MMC test plan (Ref. 2). All of the simulated cables outside of the Faraday cage (in the top part of SCATSAT) were spiral wrapped with the double sided aluminized mylar tape supplied by MMC to simulate their treatment of these cables.



RT-17507

**INTERNAL WIRE ROUTING**

- SC1-4 (ON RIB 7 BOOM) DIRECTLY INTO BAY 7 (BOX 7)
- SC2-2 (ON RIB 3 BOOM) DIRECTLY INTO BAY 3 (BOX 3)
- SC11-1 (ON RIB 4 BOOM) TO BAY 5 (BOX 5) THROUGH RIB 4
- SC6-1 (ON RIB 1 BOOM) TO BAY 6 (BOX 6) THROUGH MAIN CABLE BUNDLE.

RT-17139

**Figure 6. Boom modifications**

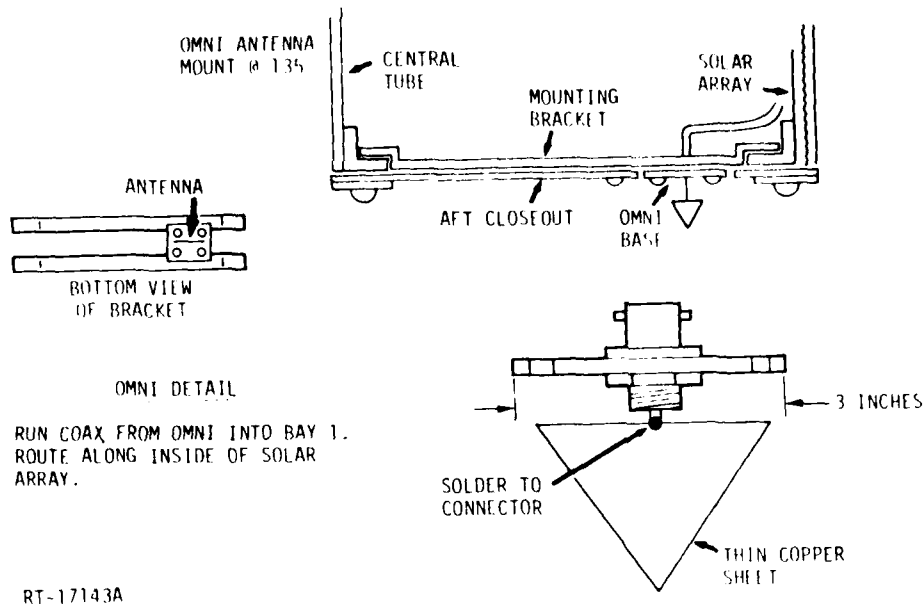


Figure 7. Aft omni antenna configuration

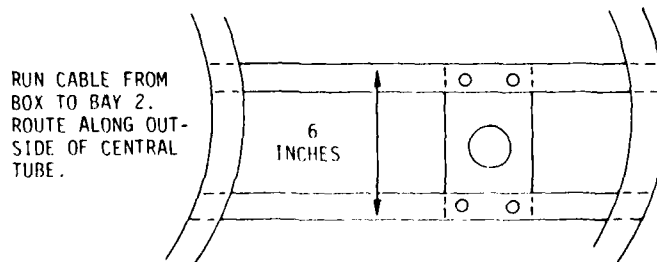
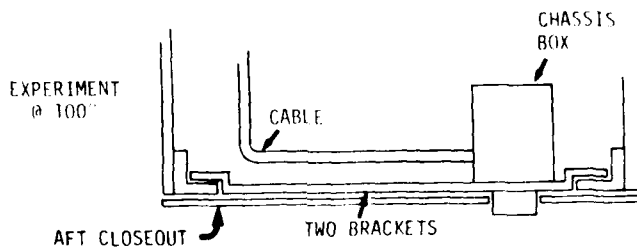
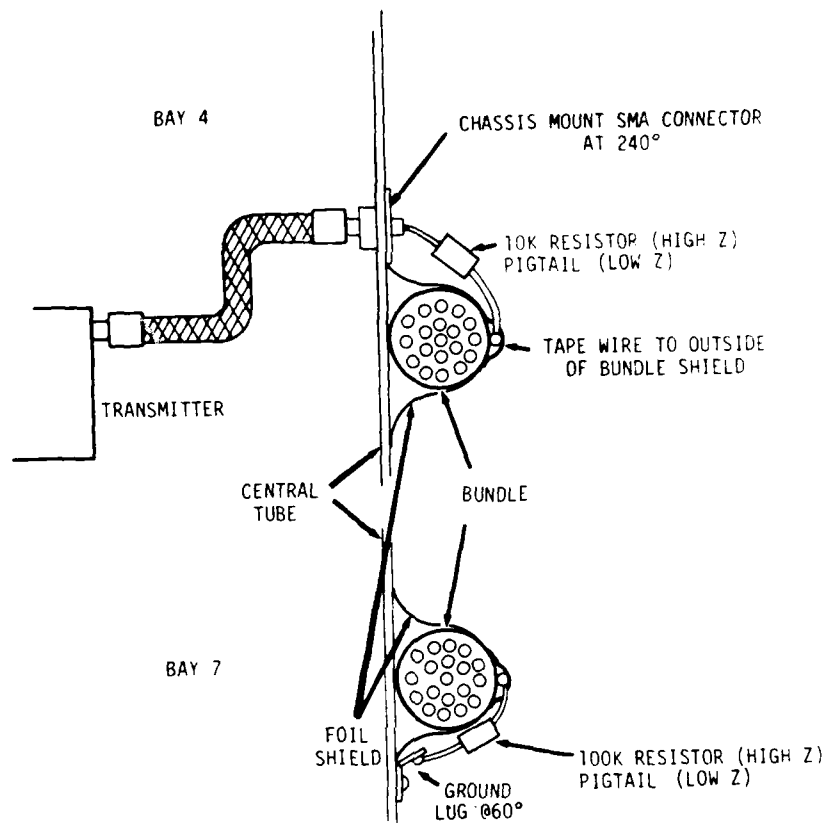
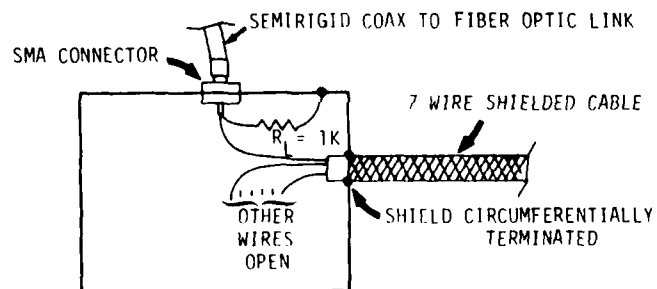


Figure 8. SC7-3 experiment configuration



RT-17136

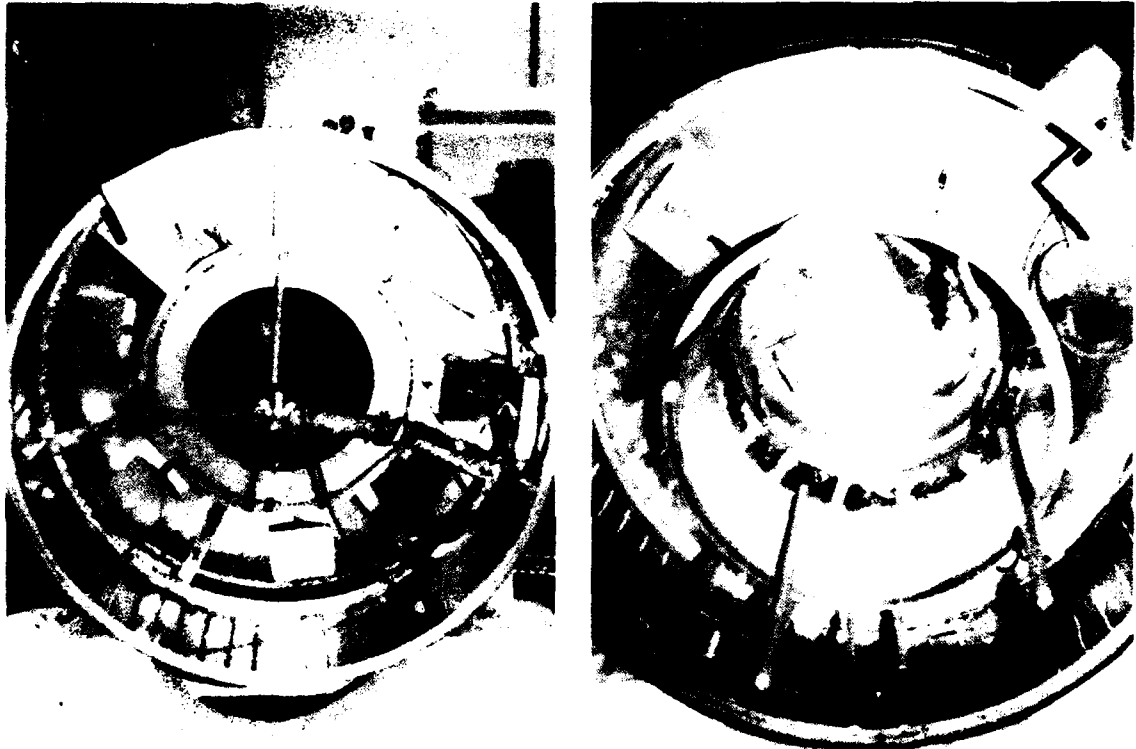
Figure 9. High and low Z TPM antenna configuration details.



RT-17158

Figure 10. Top view of box 3B/4B detail

A photo showing the top of the SCATSAT before closing appears in Figure 11(a). A photo showing the central tube and bottom of the SCATSAT appears in Figure 11(b). In the latter photo, the manhole thermal closeout, the main bundle shield, and the High and Low Z TPM antennas are in place. Installation of the aft omni antenna and SC7 experiment is also shown.



(a) Top view

(b) Bottom view

Figure 11. Internal views of SCATSAT

A special modification was made to facilitate data taking. The SCI-8B "Cable" measurement point is permanently attached to its FODL transmitter but the input to the transmitter simulating the TPM required frequent changes to monitor the various measurement points. This would have required opening and closing the belly band segment over bay 4 for each change. Instead of using this time consuming procedure, all of the measurement points and the input to the FODL transmitter were brought to a patch panel mounted on Rib 4 and accessible through a series of holes in the belly band.

This allows an external jumper to easily select the measurement point without need for opening the cover each time. This arrangement is shown schematically in Figure 12(a) and in the photo of Figure 12(b).

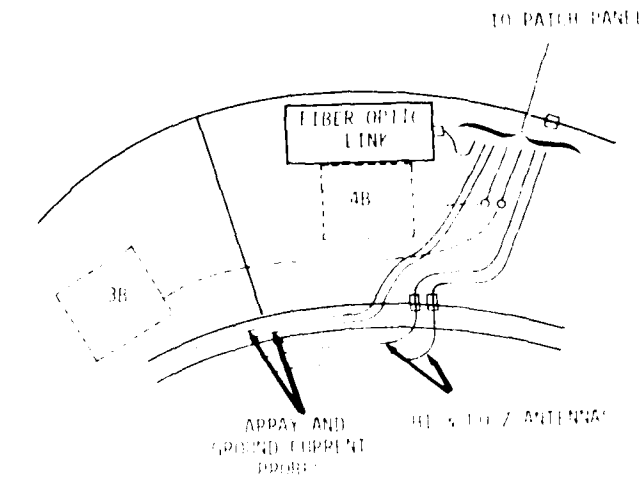
The SCATSAT was closed electromagnetically for all of the measurements. The patch panel is pulled securely against the inside of the cover door on bay 4 by screws to prevent leakage through this non-realistic modification. The jumper cable was kept short and routed against the body so as to not alter the external body configuration significantly. The jumper was semirigid coax with SMA connectors to minimize leakage.

### INJECTION POINTS AND METHODS

The basic capacitive direct injection setup is shown in Figure 13(b). The Anvil 160 pulser, a 3 inch by 4 inch by 6 inch box, is mounted at the center of a 27 inch diameter metal disc with its output connector feeding through the disc. The disc is then suspended or supported at a distance of 35 cm from the SCATSAT, as well centered over the drive point and as "parallel" or tangent to the object as possible. On an object such as this with its partially deployed booms, it is not always possible to get a perfectly centered and/or tangent installation. A thin bare wire with an empirically selected carbon composition damping resistor in it is used to attach the pulser output to an attachment point on the SCATSAT. The Anvil 160 pulser is battery powered and triggered through a fiber optic line so that the driver is completely isolated from everything but the test object. It produces the fast rising, slowly decaying pulse shown in Figure 14(a), with a peak amplitude of  $\sim 180$  V and a full width at half maximum of 50 ns.

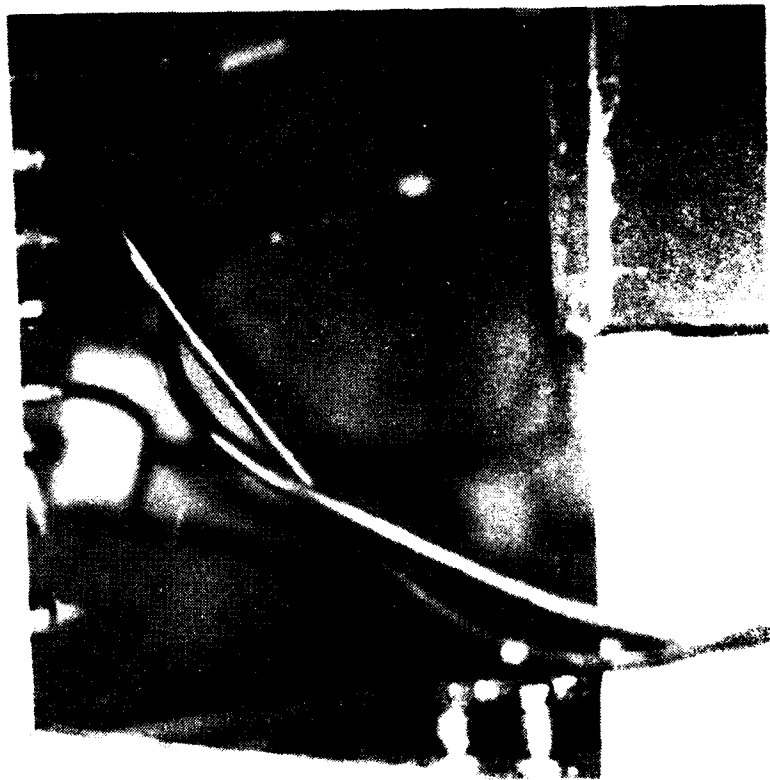
The equivalent circuit of this drive setup is a simple series R-L-C where R is the damping resistor, L is the inductance of the wire, and C is the object-to-coupler disc capacitance. With  $R = 0$  the circuit rings at a frequency determined by L and C. The resistor is chosen to be the value which just critically damps the oscillatory current to produce the single pulse shown in Figure 14(b). The result is a peak current of the order of 800 mA with a FWHM of 8 ns. The optimum resistor for this drive configuration is  $150\Omega$ . The drive current was measured with a CT2 current probe and the 30 foot semirigid coax hardwired to the oscilloscope. This current probe has a bandwidth of 10 KHz to 200 MHz, with a risetime of 0.5 ns.

Attachment points were placed on the SCATSAT, especially on flat surfaces such as the solar array or aft thermal closeout, to facilitate attachment of the CDI driver



DT 1157

(a) Top view



(b) Photo

Figure 12. Patch panel and approximate cable routing

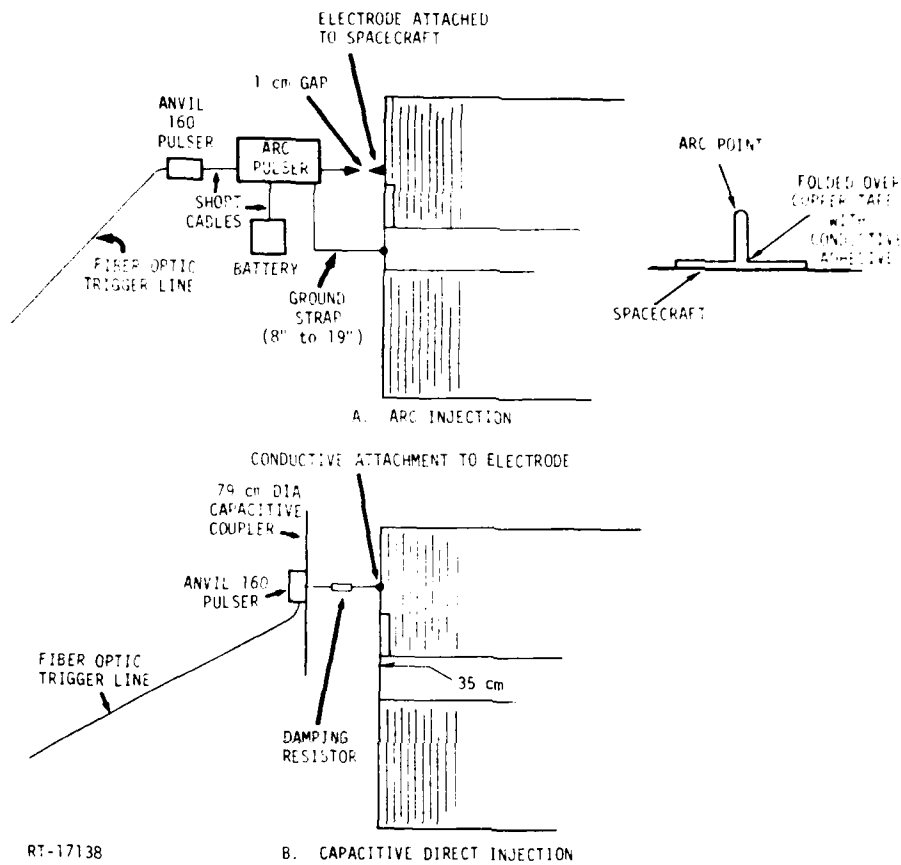


Figure 13. Examples of two injection techniques to arc point 8.

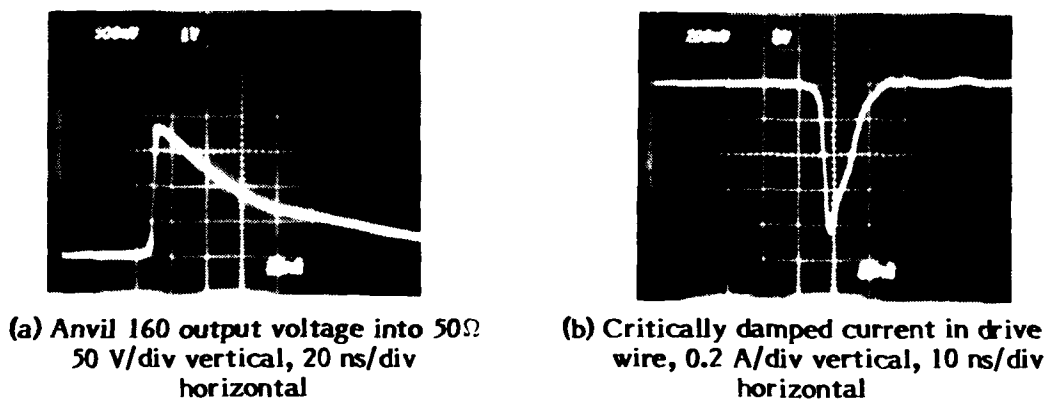
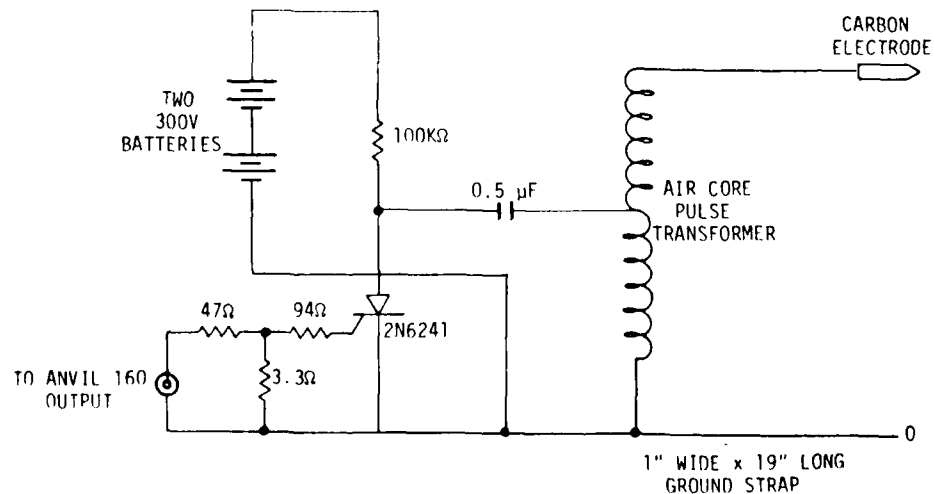


Figure 14. Capacitive direct injection waveforms

wire and to provide a well defined injection point so that both CDI and arcs were at the same point. These consisted simply of a piece of 1-inch-wide copper tape, with a conductive adhesive, doubled for about a half an inch and with about a one inch long tab on either side as shown in Figure 13(a). These were then securely taped to the SCATSAT at injection points 3, 4, 5, 6, 8, 9, and 10. Injection points 1, 2, and 7 were to the aluminum channel used to mount the booms to the SCATSAT. CDI attachment and arcs were both to the corner of these brackets. Injection point 11 was to a lug under the aft closeout screw.

### ARC INJECTION

The arc pulser was constructed basically as described in Mil Standard 1541. A schematic of our design is shown in Figure 15. The capacitor charges through the 100K $\Omega$  resistor and transformer primary to the 600 volt battery potential. The SCR is then triggered by the Anvil 160 output pulse shown in Figure 14(a), which rapidly discharges the capacitor through the transformer primary creating a high voltage on the carbon electrode. The SCR turns off after the pulse because the 100 K $\Omega$  resistor limits the anode current to less than the holding value. For the R and C values used, the pulser can be triggered at a maximum rate of 5 pps though we used a rate of 1 pps. The use of battery power and the Anvil 160 as a trigger results in an isolated pulser for the arc injection as well as for the CDI.



RT-17506

Figure 15. Arc pulser schematic diagram

The transformer caused annoying and time consuming problems. MMC used a Modoelectric\* Model B1 electronic flash trigger transformer in their pulser. We attempted to do the same, but apparently received the wrong transformer from the manufacturer as our pulser refused to arc across even the smallest gap with either of the two transformers we received. Because of the press of time, we substituted a high voltage autotransformer from a hand held Tesla coil used in leak testing of vacuum systems. This device worked quite well and would arc across a gap of up to about 15 mm.

The arc current waveform was characterized by measuring the ground strap current for a number of gap widths, with the results shown in Table 2. An example of a 10 mm waveform is shown in Figure 16. The most obvious result of this characterization is the rather large variation in peak amplitude of the arc current which is unlike the extremely repeatable CDI current. Of course, this is not unexpected since arc formation depends on uncontrollable factors. Watching the arc showed that it took a different path and went to a different point on the end of the ground strap nearly every time. There was also a noticeable jitter between the time of triggering the pulser and when the arc actually occurred. Clearly the largest amplitude and narrowest pulse occurred for the wider gap and the 10 mm gap was selected for use. The gap was measured between the pointed carbon electrode and the attachment points described earlier.

**Table 2. Arc Characteristics vs Gap Width**

Gap (mm)	Average Peak (Amps)	FWHM (ns)	Number of Pulses
3	4.5 ± 0.5*	Very wide	2
6-7	9.6 ± 3.5	18 $\begin{smallmatrix} +12 \\ -5 \end{smallmatrix}$	7
10	19 ± 6	12 ± 2	6
12	23 ± 2*	11 $\begin{smallmatrix} +1 \\ -2 \end{smallmatrix}$	3

\*Small deviation because of smaller sample size

## INJECTOR CONNECTIONS

The capacitive or arc injectors were attached to the SCATSAT as described above and at the exact locations shown in Table 3. The single wire of the CDI pulser was conductively connected to the attachment point. The electrode of the arc pulser was

\* Modelectric Products Corp., Cindy Lane (Wayside), Asbury Park, New Jersey 07712

placed 1 cm away from the attachment point and the ground strap connected at the point indicated. The gap tolerance was of the order of a mm, always on the high side. The point of the electrode sometimes had to be placed off to the side of the attachment point to be sure that the arc occurred to that point rather than to something else, e.g., the boom rather than the mounting bracket. Verification of arc to the proper point was made by watching the arc for a time as the pulser ran at a 1 pps rate.

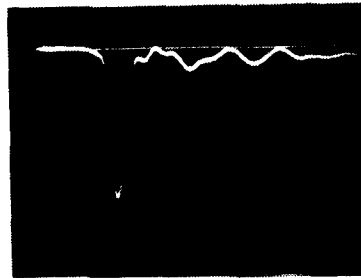


Figure 16. Sample arc current waveform

Table 3. Pulser Attachment Points

P78-2 Arc Point	SCATSAT Pulser Attachment Points	
	Arc Ground	Arc HV & CDI Wire
7	Belly band on bay 2	Base of SC6-1 boom
8	Belly band on bay 7	Array above SC1-1
9	Belly band on bay 7	Array left of SC1-1
3	Aft closeout ring (225°)	Array 4" above and right of SC10-3
5	Aft closeout ring (120°)	Base of aft omni antenna
11	Aft closeout ring (120°)	Just outside of conductive ring around SC7-3 aperture
10	Aft closeout ring (120°)	Closeout screw on SC7-3
6	Aft closeout ring (330°)	Aft closeout at ~330°
1	Belly band on bay 3	Base of SC2-2 boom
2	Top closeout ring above boom	Base of SC1-4 boom
4	Aft closeout ring near end of boom	Thermal blanket wrap on SC4-1 at end of boom

## DATA TAKING

The data taking began with capacitive direct injection only since the arc pulser was not yet available. The first six injection points, 7, 8, 9, 5, 3, and 4 in that order, were taken with both the hardwired and isolated techniques. Photos were taken at several sweep speeds to show both early high frequency content and late time behavior.

The HDL links, while more convenient to use than other isolated data links, still require careful nurturing and special attention to calibration. Prior to any data taking the links were calibrated against external as well as internal calibration sources as follows. A 50 MHz sinusoidal waveform was fed into the link while monitoring the output. The input was adjusted in amplitude until the output started to be slightly non-linear; the input and output levels were then recorded. This determined the maximum input/output signal ranges, which were not exceeded during data taking, and the system gains. The avalanche diode current was recorded and this same current maintained as close as possible in subsequent data taking since system gain is sensitive to this current. Then the output amplitude and waveform for the internal transmitter calibrator were recorded. This latter signal was the calibration routinely used during the data taking. Calibration of the internal input attenuator system was assumed correct. A recheck of the external calibration was made after all isolated data taking was completed.

The results of the calibrations are shown in Table 4. The gain of channel 5 was checked twice initially because it seemed too high and was in such poor agreement with the internal calibration (a factor of more than 5 off). After the tests were completed, another calibration was made with similar results for the external input. But at this time, a private communication with another user of the links revealed that the internal calibrators of both units had been set to new values. Using these, the post test internal calibrations are in substantially better agreement with all of the external calibrations as shown in the table.

**Table 4. Results of FODL Calibration**

When	Channel	External Input	Internal Calibrator
Pretest	5	24	4.8*
After CDI 7	5	25	---
Post test	5	28	36**
Pretest	15	9.8	5.4*
Post test	15	9.2	12**

\*Based on calibration signals recorded in transmitters by HDL

\*\*Based on calibration signals reported by Dave Fromme, Mission Research Corporation, San Diego.

Data taking on the first six capacitive injections proceeded slowly even though the data links were quite well behaved. At the end of these first six tests the hardwire and isolated data were compared for peak amplitudes, frequency content, and general waveshape agreement. The agreement was quite good in all respects, with the major

difference being some slight loss of high frequency content in the isolated data. The hardware data was of far superior quality as the result of much better signal to noise ratio. This combined with the apparent lack of effect of the hardware on the measurement waveforms and the great time savings afforded by not using the data links resulted in a decision to discontinue their use for all subsequent measurements. The last five capacitive injections were then completed.

Before and after each of the injection set ups, i.e. at each of the eleven points, the drive current waveform was recorded on film. As already mentioned, this was quite repeatable and well behaved. The only difficulty occurred at drive point 4. Here, rather than driving to a simple body as is the case elsewhere, we are driving the end of a boom which, though folded against the body, is not in direct contact with it except through the inductance of 104 inches of cable. This alters the drive circuit considerably. Several damping resistors were tried in an attempt to obtain a cleaner waveform without great success. The best compromise was a  $510\Omega$  resistor which produced the waveform shown in Figure 17.

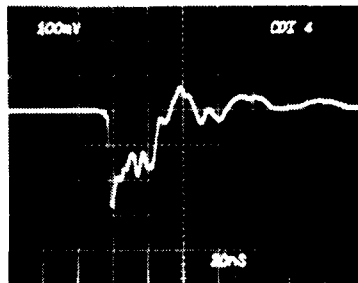


Figure 17. CDI current waveform at point 4 only, 100 mA/div vertical, 20 ns/div horizontal

Also before and after each set of isolated measurements, internal fiber optic calibrations were taken to check system gain and battery condition. The batteries performed well. Only once was a low battery discovered and this was before the test so that no data were lost.

The arc injections were started immediately after the capacitive injection were completed. The procedure used was somewhat different in that basically single pulse operation was used rather than the 1000 pps repetition rate of CDI and several shots had to be taken at each point to bound the variation in amplitude as the arc amplitude varied. To avoid recording of anomalously low responses which sometimes occurred, a technique was adopted of watching a number of responses to get a feel for what it

should be, then photographing a response and rejecting it if it was not representative of the average of a number of observations. At least three responses were photographed for each measurement except for the PCU Ground and Upper Array responses which were generally quite stable even with arc variation.

The effect of the ground point location on measured responses was tested by varying the ground attachment point to the SCATSAT for the first two arc points, 8 and 2. The attachment points were to either the belly band closeout screws on a rib or to the top thermal closeout. The average variation was less than a factor of 1.5 with a maximum of about 3.

The data are presented and discussed in detail in the next section.

### 3. RESULTS

The results of the SCATSAT experimental effort, the available results from P78-2 injections, and calculations based on these data sets are presented in this section.

#### P78-2 RESULTS

During the arc injection tests conducted on the P78-2 spacecraft as a part of EMI/EMC testing, the Transient Pulse Monitor (TPM) and the SCI-8B Pulse Analysis experiments recorded signals induced by the arcs at the five points listed in Table 1. The results of these tests were summarized in References 4 and 5. In order to use these data to make meaningful comparisons to the SCATSAT results, all of the results must be normalized to the same level. We will use 1 ampere as the normalized drive pulse. This is valid because we are comparing electrical excitations which are expected to scale linearly with source amplitude for pulses of the same shape. The arc injection signal used by Martin Marietta was described partially in Reference 8. This paper gave the energy and time history of the pulse. Two different methods were used to calculate the corresponding peak current amplitude, yielding 30 and 50 amperes. We have therefore used the average of 40 amperes for normalizing the data and expect an uncertainty of no more than 25 percent.

The P78-2 Array and Ground data required some additional manipulation to be consistent with the SCATSAT data. First of all, the P78-2 array measurement recorded current on one of two parallel wires and the P78-2 ground recorded data on one of seven parallel wires. The corresponding measurement in SCATSAT were each on single wire simulating the P78-2 configuration. Therefore, the SCATSAT results measure the total current at these points, not one-half or one seventh as in the P78-2. The P78-2 results have been multiplied by two for array and seven for ground to be consistent with SCATSAT. Secondly, the transfer impedance of the current probes used in SCATSAT are four ohms and so the P78-2 data, which are in mA, have been multiplied by four to give the results in mV consistent with SCATSAT data.

The normalized positive and negative peak amplitudes of the four measurement points monitored by the TPM are tabulated in Table 5. Peak amplitude data only are

available for these measurements and not all injection points yielded data. The data for the SC1-8B cable antenna are shown in Table 6. This experiment had a threshold of 1.27 volts (32 mV normalized), which when exceeded, initiated logarithmically spaced time samples starting with the threshold point as zero time. Additional samples were then taken at 7, 37, 97, and 217 ns. The threshold value was the greatest positive value recorded in all cases so this measurement shows absolutely no variation with arc injection point. In five of these there were no data after the threshold value while four had smaller positive and/or negative values later on.

**Table 5. P78-2 Response Data\***

Drive Point	Measurement Point and Response Amplitude (mV)							
	PCU Ground		Upper Array		Hi Z		Lo Z	
	+	-	+	-	+	-	+	-
1	---	---	2.4	2.0	---	---	---	---
2	---	---	---	---	---	---	3.1	2.6
3	72	66	6.8	8.2	---	---	2.7	3.2
4	---	---	2.4	3.4	---	---	3.1	5.8
5	64	80	5.4	6.7	0.20	---	7.9	6.5
6	64	97	6.6	8.6	0.20	---	7.3	5.6
7	---	---	2.6	3.8	0.32	0.24	9.2	6.1
8	66	100	5.0	8.6	0.68	0.60	20.0	25.0
9	100	160	7.0	9.3	0.42	0.31	14.0	15.0
10	83	135	5.6	9.6	0.37	0.35	12.0	8.8
11	---	86	4.8	6.6	---	---	9.5	8.5

\* Normalized to 1A peak drive current

**Table 6. P78-2 SC1-8B Cable Responses\***

Arc	Location	Amplitude, mV @ Time, ns				
		0	7	37	97	217
1	SC2-2 Base	0	0	0	0	0
2	SC1-4 Base	32	0	0	0	0
3	Near SC10-3 Exit Hole	0	0	0	0	0
4	SC11 Thermal Blanket	32	0	0	0	0
5	Base of Aft Omni Antenna	32	0	0	0	0
6	Structure Adj to SC2-4 Aperture	32	0	0	0	0
7	Base of SC6-1 Boom	32	0	0	0	0
8	Solar Array Near SC1-1 BR Cover	32	+22	-22	-50	-22
9	Solar Array Near SC1-1 BR Cover	32	+22	-22	-22	0
10	Nearest Point to Conductive Ring (SC7)	32	0	-22	0	0
11	SC7 Aft Closure Screw Closet to SC7 Aperture	32	0	-22	0	0

\* Normalized to 1A peak drive current

## SCATSAT RESULTS

The SCATSAT results were recorded as time histories on oscilloscope photos. About six hundred photos were taken and it is not particularly useful to present all of them here. Instead, we will present sample data sets, tabulations of frequency content, and plots of the peak amplitudes.

As examples, Figures 18 through 25 present complete sets of data photos for CDI and arc injection at four points: on the solar array, on the central structure near the belly band, the aft end of the SCATSAT, and at the end of the undeployed SC11-1 boom. These photos are for the hardwired configuration with only one exception and are not normalized. Only one sweep speed is shown except for the upper array or PCU ground where two sweep speeds are sometimes required to show the whole waveform with sufficient detail.

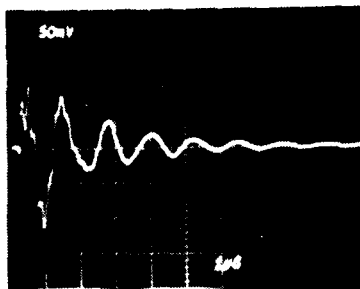
A few specific comments are in order about some of the photos or sets.

The data for injection point 9 are for injection at the same area but to different points. The CDI data are for injection directly to the conductive strips which represent the solar cells. The arc data are for an arc to the conductive strip around the edge of the SC1-1 cutout in the solar array substrate. This is shown in Figure 26. None of the arcs were directly to SC1-1 however.

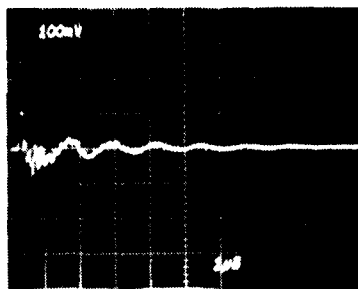
Array data has been shown at two sweep speeds in Figure 21 to show the early time high frequency which is representative of that on both the array and PCU ground measurements. The same is true in Figure 23 where two sweep speeds are shown for PCU ground data.

In Figure 24, the slower sweep speed data for PCU ground and array show a second excitation beginning about 3  $\mu$ sec after the initial excitation. This is a peculiarity of the particular Anvil 160 pulser used. It tends to trigger, not always, but frequently, on the trailing as well as the leading edge of the 3  $\mu$ sec wide laser trigger pulse. This doesn't show up in the other CDI results because the smaller damping resistor allows the energy storage capacitor in the Anvil 160 to discharge sufficiently that the output switch will not turn on. At CDI 4, the damping resistor is much larger resulting in less than full discharge of the capacitor and the resultant second output.

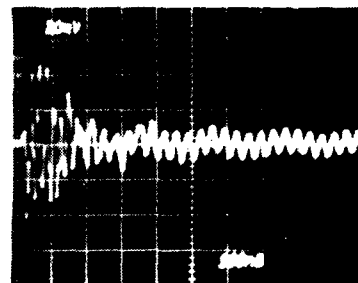
Figure 27 shows a set of data for isolated response measurements at point 4 for CDI. Five additional sets of CDI data were taken with the isolated instrumentation setup but are not presented except in tabular form later on. Amplitudes, frequency content, and general waveform agreement for all six data sets have been compared with the conclusion that there are no significant differences. This is not surprising since the



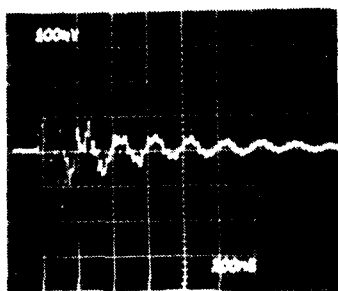
Position: Ground  
 Vertical: 50 mV/div  
 Horizontal: 1 μs/div



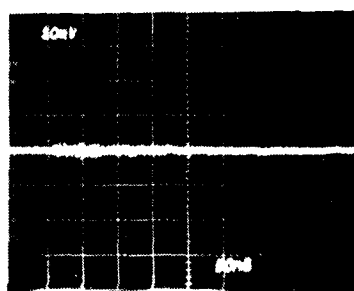
Position: Array  
 Vertical: 100 mV/div  
 Horizontal: 1 μs/div



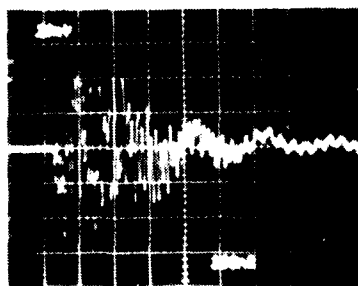
Position: 4B  
 Vertical: 1 mV/div  
 Horizontal: 100 ns/div



Position: 3B  
 Vertical: 5 mV/div  
 Horizontal: 200 ns/div



Position: Hi Z  
 Vertical: 0.5 mV/div  
 Horizontal: 50 ns/div



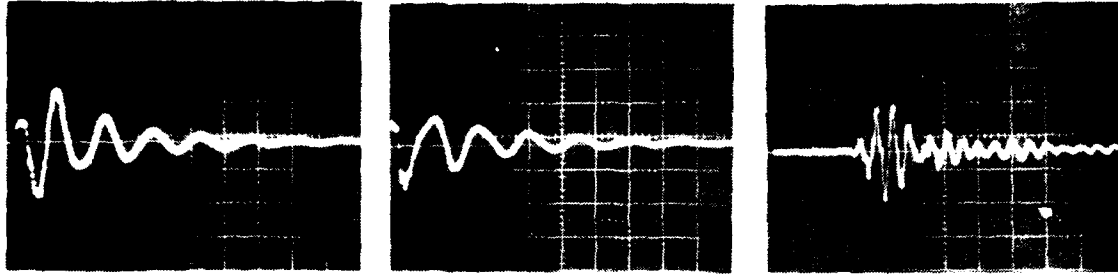
Position: Lo Z  
 Vertical: 1 mV/div  
 Horizontal: 100 ns/div



Position: Cable\*  
 Vertical: 8 mV/div  
 Horizontal: 50 ns/div

\* Isolated

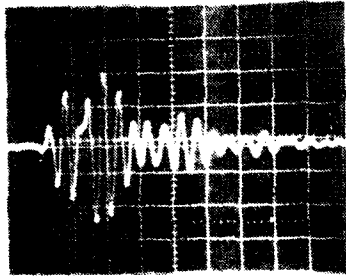
Figure 18. CDI response waveforms for injection at point 9 on solar array



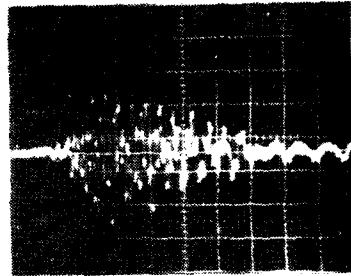
Position: Ground  
 Vertical: 100 mV/div  
 Horizontal: 1 μs/div

Position: Array  
 Vertical: 50 mV/div  
 Horizontal: 1 μs/div

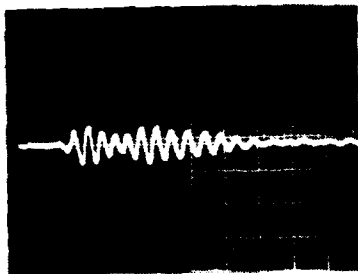
Position: 4B  
 Vertical: 10 mV/div  
 Horizontal: 50 ns/div



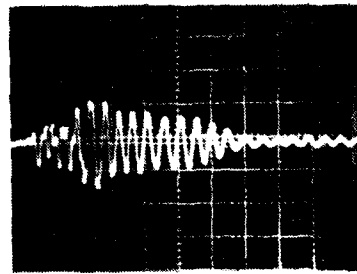
Position: 3B  
 Vertical: 100 mV/div  
 Horizontal: 50 ns/div



Position: Hi Z  
 Vertical: 0.5 mV/div  
 Horizontal: 50 ns/div

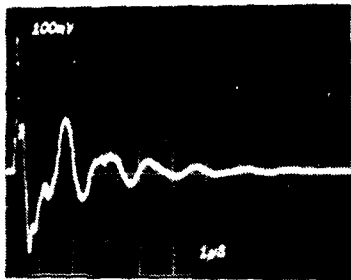


Position: Lo Z  
 Vertical: 50 mV/div  
 Horizontal: 50 ns/div

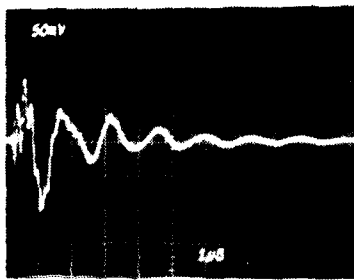


Position: Cable  
 Vertical: 200 mV/div  
 Horizontal: 50 ns/div

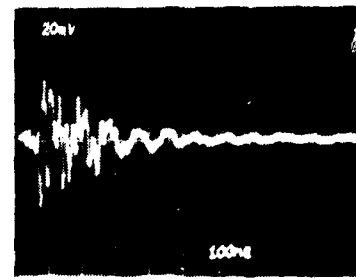
Figure 19. Arc injection response waveforms for injection at point 9 to the solar array substrate



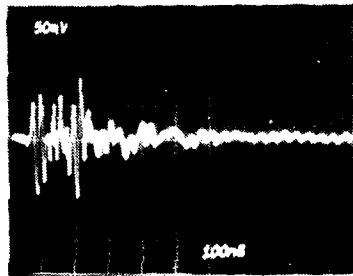
Position: Ground  
 Vertical: 5 mV/div  
 Horizontal: 1  $\mu$ s/div



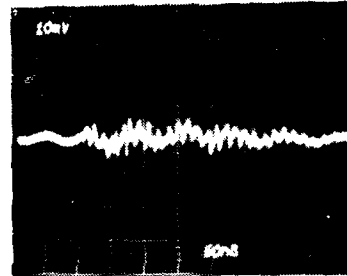
Position: Array  
 Vertical: 2.5 mV/div  
 Horizontal: 1  $\mu$ s/div



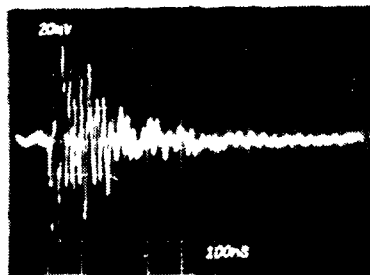
Position: 4B  
 Vertical: 1 mV/div  
 Horizontal: 100 ns/div



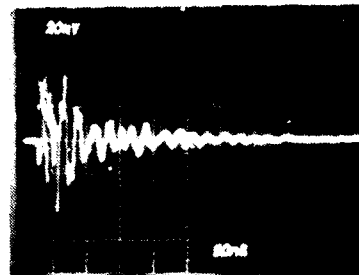
Position: 3B  
 Vertical: 2.5 mV/div  
 Horizontal: 100 ns/div



Position: Hi Z  
 Vertical: 0.5 mV/div  
 Horizontal: 50 ns/div

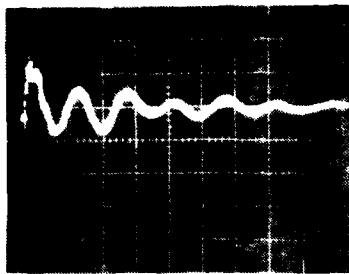


Position: Lo Z  
 Vertical: 1 mV/div  
 Horizontal: 100 ns/div

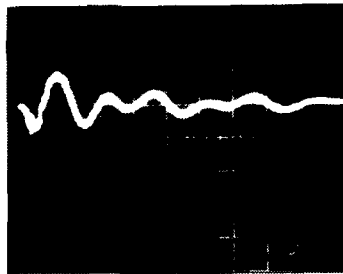


Position: Cable  
 Vertical: 1 mV/div  
 Horizontal: 50 ns/div

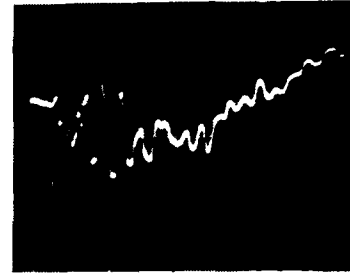
Figure 20. CDI response waveforms for injection at point 2 on central structure



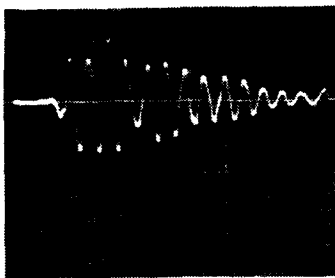
Position: Ground  
 Vertical: 50 mV/div  
 Horizontal: 0.5  $\mu$ s/div



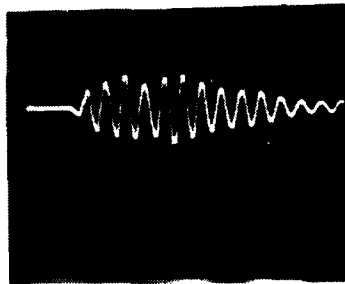
Position: Array  
 Vertical: 20 mV/div  
 Horizontal: 0.5  $\mu$ s/div



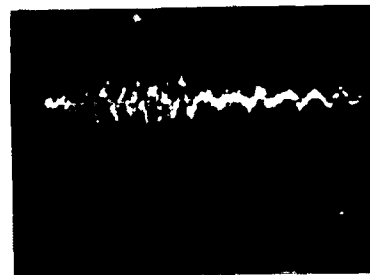
Position: Array (Again)  
 Vertical: 10 mV/div  
 Horizontal: 50 ns/div



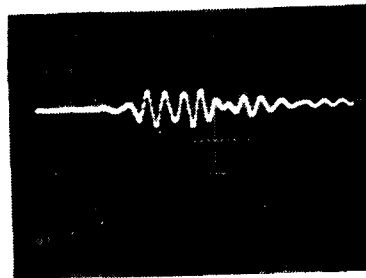
Position: 4B  
 Vertical: 10 mV/div  
 Horizontal: 50 ns/div



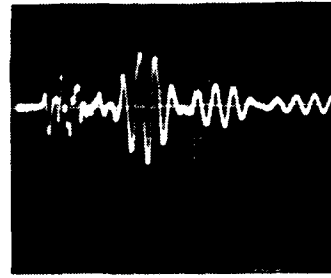
Position: 3B  
 Vertical: 20 mV/div  
 Horizontal: 50 ns/div



Position: Hi Z  
 Vertical: 0.5 mV/div  
 Horizontal: 50 ns/div

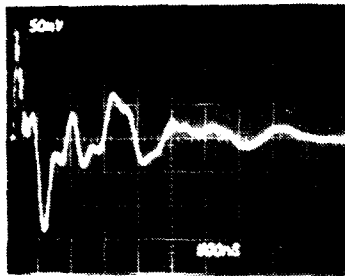


Position: Lo Z  
 Vertical: 20 mV/div  
 Horizontal: 50 ns/div

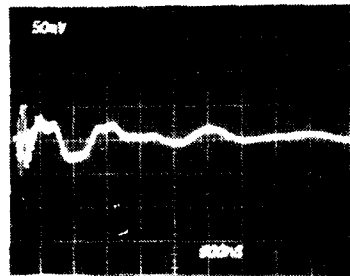


Position: Cable  
 Vertical: 100 mV/div  
 Horizontal: 50 ns/div

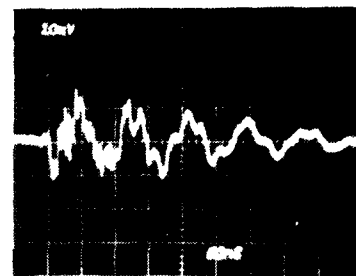
Figure 21. Arc injection response waveforms for injection at point 2 on central structure



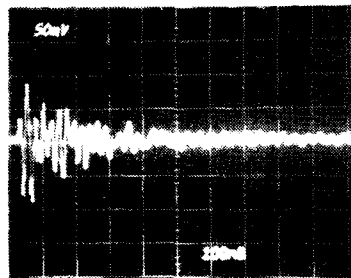
Position: Ground  
 Vertical: 2.5 mV/div  
 Horizontal: 0.5  $\mu$ s/div



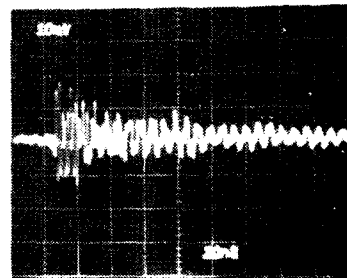
Position: Array  
 Vertical: 2.5 mV/div  
 Horizontal: 0.5  $\mu$ s/div



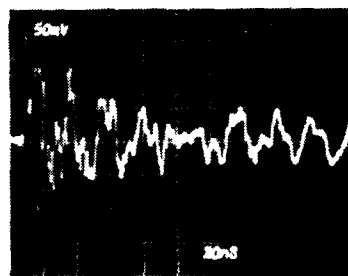
Position: 4B  
 Vertical: 0.5 mV/div  
 Horizontal: 50 ns/div



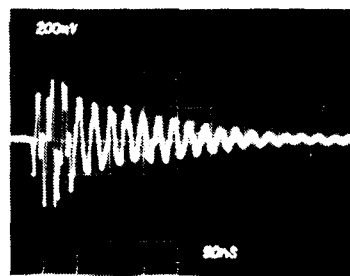
Position: 3B  
 Vertical: 2.5 mV/div  
 Horizontal: 100 ns/div



Position: Hi Z  
 Vertical: 0.5 mV/div  
 Horizontal: 20 ns/div

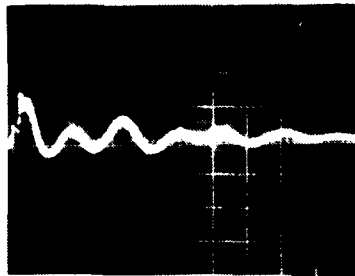


Position: Lo Z  
 Vertical: 2.5 mV/div  
 Horizontal: 20 ns/div

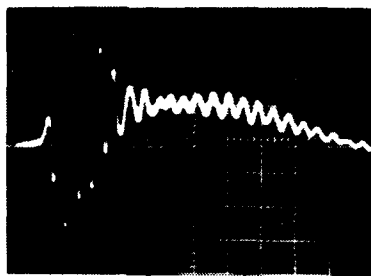


Position: Cable  
 Vertical: 10 mV/div  
 Horizontal: 50 ns/div

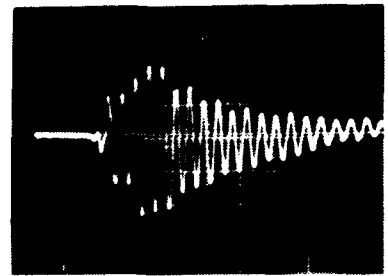
Figure 22. CDI response waveforms for injection at point 11 on aft end



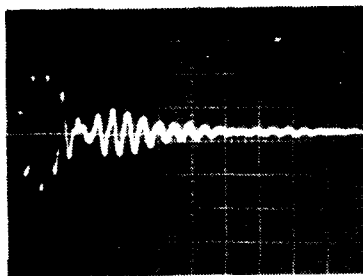
Position: Ground  
Vertical: 20 mV/div  
Horizontal: 0.5  $\mu$ s/div



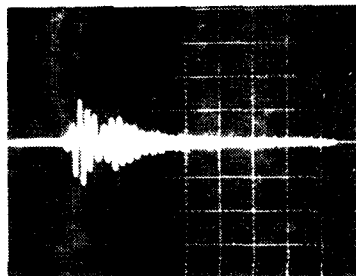
Position: Ground (Again)  
Vertical: 20 mV/div  
Horizontal: 50 ns/div



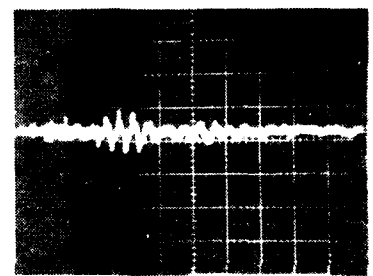
Position: Array  
Vertical: 20 mV/div  
Horizontal: 50 ns/div



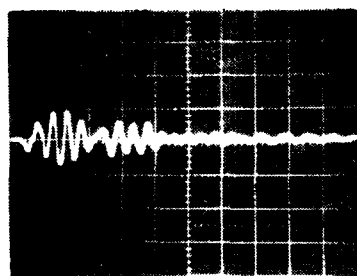
Position: 4B  
Vertical: 10 mV/div  
Horizontal: 50 ns/div



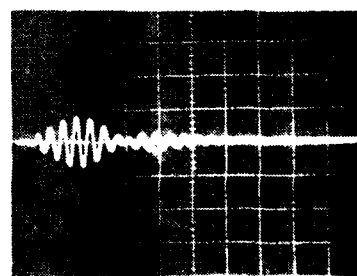
Position: 3B  
Vertical: 100 mV/div  
Horizontal: 100 ns/div



Position: Hi Z  
Vertical: 0.5 mV/div  
Horizontal: 50 ns/div

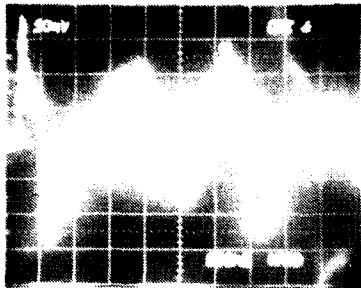


Position: Lo Z  
Vertical: 20 mV/div  
Horizontal: 50 ns/div

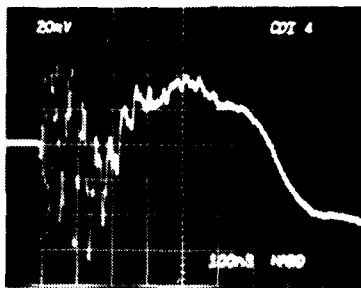


Position: Cable  
Vertical: 200 mV/div  
Horizontal: 50 ns/div

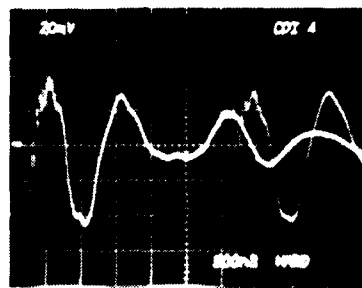
Figure 23. Arc injection response waveforms for injection at point 11 on aft end



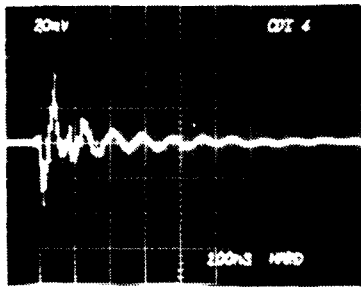
Position: Ground  
Vertical: 2.5 mV/div  
Horizontal: 0.5 µs/div



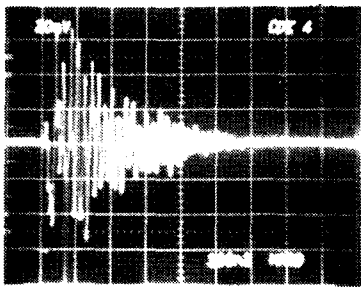
Position: Array  
Vertical: 1 mV/div  
Horizontal: 100 ns/div



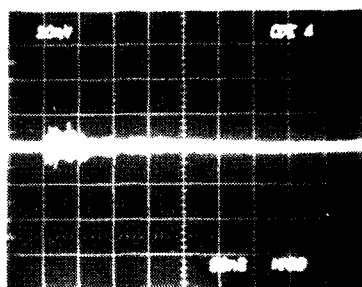
Position: Array (Again)  
Vertical: 1 mV/div  
Horizontal: 0.5 µs/div



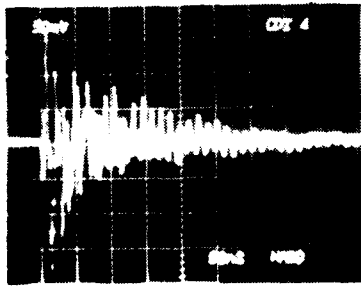
Position: 4B  
Vertical: 1 mV/div  
Horizontal: 100 ns/div



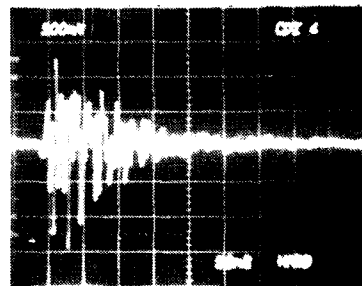
Position: 3B  
Vertical: 1 mV/div  
Horizontal: 100 ns/div



Position: Hi Z  
Vertical: 0.5 mV/div  
Horizontal: 50 ns/div

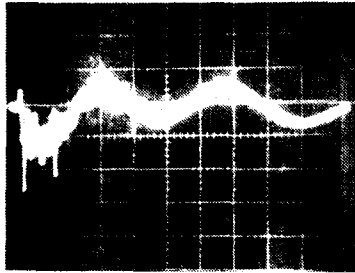


Position: Lo Z  
Vertical: 2.5 mV/div  
Horizontal: 50 ns/div

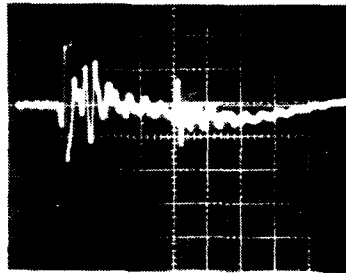


Position: Cable  
Vertical: 5 mV/div  
Horizontal: 50 ns/div

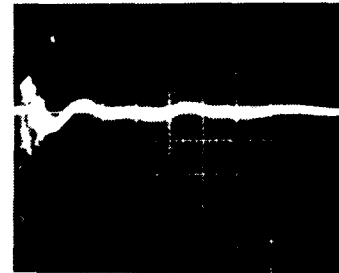
Figure 24. CDI response waveforms for injection at point 4 on end of SC11-1 boom



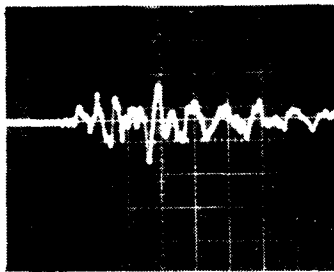
Position: Ground  
 Vertical: 50 mV/div  
 Horizontal: 0.2  $\mu$ s/div



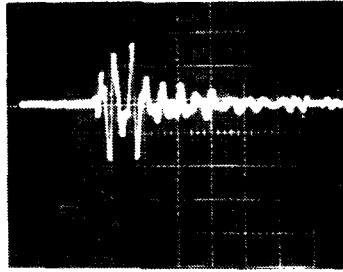
Position: Array  
 Vertical: 50 mV/div  
 Horizontal: 100 ns/div



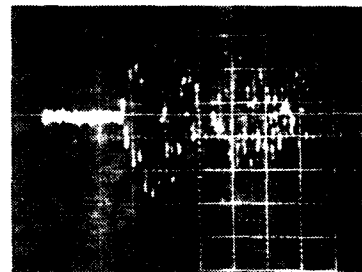
Position: Array (Again)  
 Vertical: 50 mV/div  
 Horizontal: 0.5  $\mu$ s/div



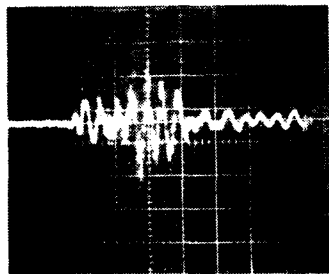
Position: 4B  
 Vertical: 10 mV/div  
 Horizontal: 50 ns/div



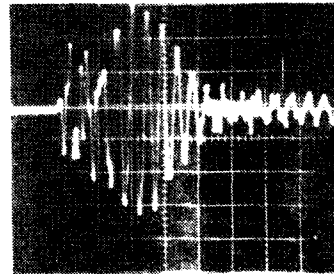
Position: 3B  
 Vertical: 50 mV/div  
 Horizontal: 100 ns/div



Position: Hi Z  
 Vertical: 0.5 mV/div  
 Horizontal: 50 ns/div



Position: Lo Z  
 Vertical: 10 mV/div  
 Horizontal: 50 ns/div



Position: Cable  
 Vertical: 100 mV/div  
 Horizontal: 50 ns/div

Figure 25. Arc injection response waveforms for injection at point 4 on end of SC11-1 boom

effect of the hardware is to disturb external surface currents in the vicinity of the wire attachment point. The internal measurements will not be affected unless the dominant point of entry is in the vicinity of the disturbed currents, i.e., near the attachment point, and then only if the disturbance is large. For six of the seven measurements, the attachment point was not closer than 50 cm from the nearest injection point. For the seventh, the attachment point was 20 cm from three injection points but at least 50 cm from the other eight. The current flowing on the hardware was measured and had a peak of 100 mA with a rise time of 25 ns. Thus, at the closest injection point, the rate of change of surface current is of the order of

$$\dot{j} = \frac{0.1 \text{ A}}{2\pi(0.2 \text{ m}) 25 \times 10^{-9} \text{ sec}} = 0.32 \text{ A/m-s} \quad .$$

External surface current measurements for CDI range from two to three orders of magnitude greater than this (Ref. 7) and so it is reasonable that the effect of the hardware is negligible. Comparison of Figures 24 and 27 also show good agreement and the superior quality of the hardwired data.

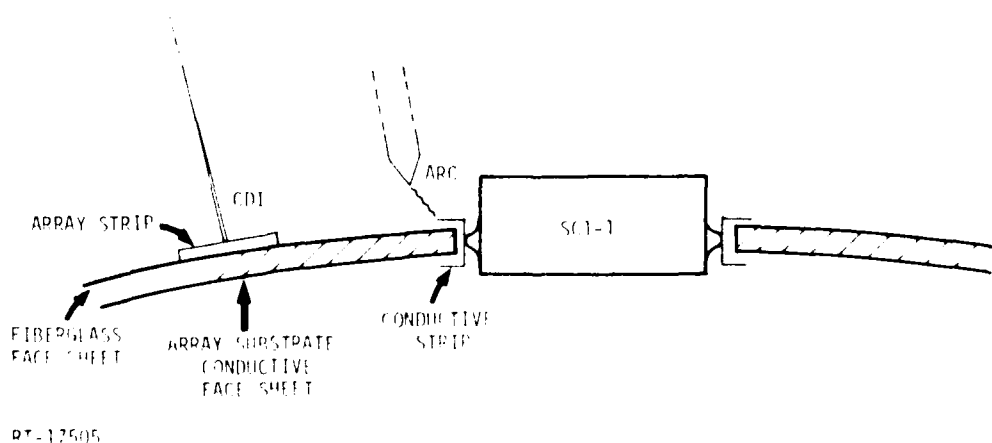
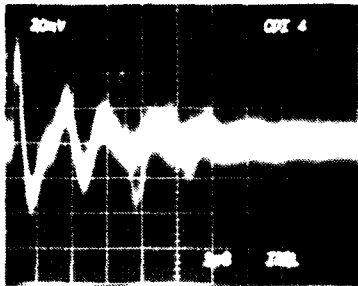
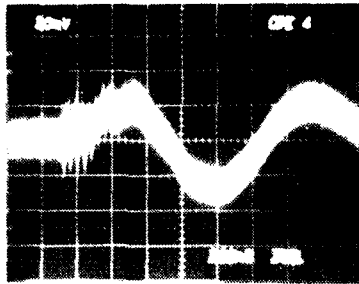


Figure 26. Detail of injection point 9

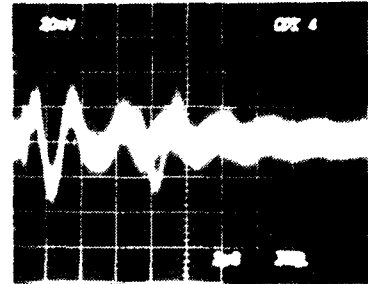
There is another important consideration on use of a hardwired data taking scheme. In addition to disturbance of the object surface currents, leakage of signals through the hardware cable itself must be considered. We used a semirigid cable, i.e., solid outer shield, with SMA connectors to minimize leakage at the cable ends. The importance of low leakage can be shown by a simple calculation and an example. If the



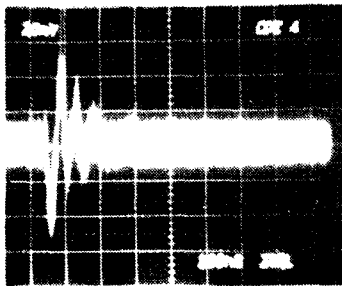
Position: Ground  
Vertical: 6.6 mV/div  
Horizontal: 1  $\mu$ s/div



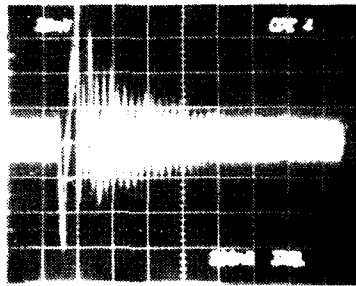
Position: Array  
Vertical: 3.3 mV/div  
Horizontal: 200 ns/div



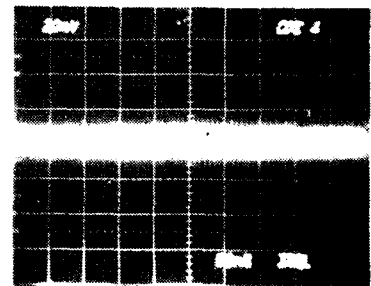
Position: Array (Again)  
Vertical: 3.3 mV/div  
Horizontal: 1  $\mu$ s/div



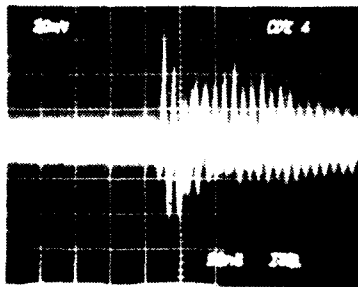
Position: 4B  
Vertical: 0.83 mV/div  
Horizontal: 100 ns/div



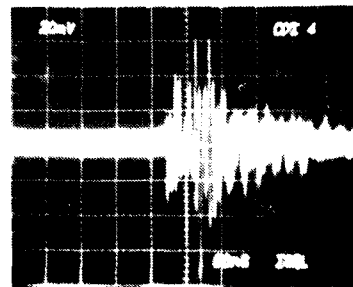
Position: 3B  
Vertical: 1.66 mV/div  
Horizontal: 100 ns/div



Position: Hi Z  
Vertical: 0.83 mV/div  
Horizontal: 50 ns/div



Position: Lo Z  
Vertical: 3.3 mV/div  
Horizontal: 50 ns/div



Position: Cable  
Vertical: 4 mV/div  
Horizontal: 50 ns/div

Figure 27. Isolated CDI response waveforms for injection at point 4

cable were braided RG-58/u rather than semirigid coax, the signal on the center wire due to leakage of the shield current would be

$$\begin{aligned}V_L &= Z_T(\Omega/m @ f) \times I_s @ f \times L (m) \\&= (0.04\Omega^*/m @ 4 \text{ MHz}) (0.1A @ 4 \text{ MHz}^{**}) (9 m) \\&= 36 \text{ mV} .\end{aligned}$$

The signals of interest are generally in the range 0.1 to 10 mV with only a couple going to 10's of mV. Thus, leakage signals due to current on the instrumentation wire shield would mask the signals of interest if an RG 58/u were used. Leakage at connectors can further add to leakage signals. During this experiment, even using semirigid coax, we experienced intermittent leakage through a faulty SMA connector at the screen room end of the semirigid coax and had to ground the shield ahead of the connector to reduce current flow across the connector and then wrap it to further reduce leakage. These techniques reduced the leakage to negligible levels, but point out graphically the need for a low leakage hardwire scheme.

The frequencies appearing in each measurement have been determined by visual examination of the photographs. They are tabulated in Table 7. Ways to reduce this massive table were examined, but in general there is not enough commonality of frequencies to justify a summary. And it is likely that differences for a given measurement point as the drive location is varied are the result of different points of entry being excited and so the differences are of importance. Both hardwired and isolated data are presented for six of the CDI drive points for comparison. More will be said about the frequencies in the comparisons to be made in the next section.

The normalized peak amplitudes of SCATSAT responses are presented in Figures 28 through 38 along with the normalized P78-2 data. The data are plotted so that all the responses for a given injection point are presented together to facilitate comparisons. Some comments are in order about the normalization procedure before the results are discussed in the next section.

---

\* Ref. 9 and others.

\*\* The measured ringing frequency and current on the cable.

**Table 7. Frequencies in MHz Observed in SCATSAT Measurements**

Measurement Point	Hardwire CDI 1	Hardwire CDI 2	Hardwire CDI 7	Isolated CDI 7
PCU Gnd	Tiny ~50 and ~200 early, 0.71 dominant	Early 2.5 to 5 on 0.71 dominant	Small 50 on 5 on 0.79 late	Small 50 early, 0.9-0.77 late
Upper Array	50 and higher early, ~5 mid, 0.71 late and domi-	Tiny 50 on larger 5 on dominant 0.71	Larger 49 early with 5.6 then 0.79 late	Larger 50 early, 0.79 late and dominant
4B Load	11 dominant, large 50 early	Early 50 on 13	~60 and 130 early, 29 late	120 early, 30-40 late
3B Load	50 dominant early, 40 late	44 dominant mixed with L.F.	50 early, 29 late	46 early, 30 late
Hi Z	67 dominant	69 dominant	130 early, 27 late	130 early, 27 late
Lo Z	46 dominant	50 dominant	40-50 and 130 early, 29 late	80 early, 28 late
Cable	50 early, 40 late	50 dominant	Small 170 early, 45 dominant	Small 150-200 early 45 dominant
Measurement Point	Hardwire CDI 3	Isolated CDI 3	Hardwire CDI 8	Isolated CDI 8
PCU Gnd	Early 15, then 6.4 on ~1.3 late	Early 15, then 6.7, 1.3 1.3 late	Very small 67 early, One cycle of 4.2 0.77 late, dominant	Very small 67 early Some 5 MHz, then 0.79 late, dominant
Upper Array	Few cycles 17 on 1.3	Few cycles 16, 1.2 later	Small 67 early, One cycle 14 1.5 $\mu$ s of 5, 0.77 late, dominant	Small 56 early, One cycle 14 1.5 $\mu$ s of 5 0.75 late, dominant
4B Load	Early 130, 42-44 dominant, small 9.5	Early 130, then 27 on 9.2	170 early, ~50 dominant	140 early, 47 dominant small 5 late
3B Load	Early ~200, then 40-50, small 6.3 late	Small 130, then 40-45 on ~7	Very small 140 early ~50 burst, 5 late	Negligible 140, 45-48 burst, 5 late
Hi Z	130-140, small 25 late	Not discernible	150	140
Lo Z	146 dominant on small 40	140 on small ~40	180-200 early, Complex burst of 40-50, small 5	Small 140 early 45-48 burst small 5 late
Cable	150 early, 42-44 dominant	~200 early, then 43-44	Not Measured	Small 200 early 50 burst, 42 later
Measurement Point	Hardwire CDI @ 9	Isolated CDI @ 9	Hardwire CDI @ 5	Isolated CDI @ 5
PCU Gnd	Tiny 70, 5.9 for ~1 $\mu$ s, 0.79 late	Tiny 90 early, 5 for ~1 $\mu$ s, 0.71 late	Tiny 200 early, 45 on little bit of 4.5 then 0.7 later	Tiny 45, 1-2 cycles 1.6, 0.67 later
Upper Array	5.3 early on 0.75 later	Tiny 60 early, 4.8 for ~1.5 $\mu$ s, 0.71 late	Small 200 early, 47 on 1.2, then 0.71	46 early 0.71 later
4B Load	44 in a burst, then 29 on small 5	Early 170, 50 in a burst, then on late 4.5	Early 170, then ~50 changing to 29. Small 2	~100±
3B Load	47 burst, small 29 on larger 5	Small 170 early, burst of 48, later 4.5	47 burst, 29 late	Tiny 150, 44 burst, 29 later
H. Z	~170	~160	~250	Indistinguishable
Lo Z	Early 170, then 77 on 5 on small 6.7	Small 140 early, 50 in burst, small 8 late	Early VHF, burst of 70, 29 later	200 early, burst of 74, small 29 late
Cable	Not Measured	Early 220, 45 in burst, 42 later	140 early 42 later	160 early 44 later

**Table 7. Frequencies in MHz Observed in SCATSAT Measurements (continued)**

Measurement Point	Hardwire CDI 6	Hardwire CDI 10	Hardwire CDI 11
PCI Gnd	Small 60-70 early, 1.8 changing to ~1	Small 43 early, then 4 changing to ~1	Early 44 small, then 1.8 to ~1 late
Upper Array	Early 50 and Higher Freq dominant, ~0.7 later	Dominant 47 with ~160 early, ~1.1 late	Early 44-50 dominant with some ~200, ~1 late
4B Load	200, 30, ~10	12 dominant with early HF	11 dominant, some early 50 and 200
3B Load	50 early, 44 later with ~200	~45 early, 28 late	43 early, 22 late
Hi Z	Mostly ~300	400-500 early, ~140 later	140 late, 100's early
Lo Z	42 late, but 100's early, very complex	45 dominant with 100's early	42 late, 100's early
Cable	50 early, 42 late, some H.F.	43 dominant with early higher freq	43 dominant, some early 200
Measurement Point	Hardwire CDI 4	Isolated CDI 4	
PCI Gnd	Small ~70 early 0.73 dominant	Tiny 200, some 25, larger 4 to ~1.5 $\mu$ s, ~1 MHz dominant	
Upper Array	Small 160 early, 25 for ~0.4 $\mu$ s, 0.70 dominant	170 early on large 25, then 0.83 late, (LF unstable)	
4B Load	22 dominant with ~250 unit, small 100 late	180 early on ~17 for 2 cycles, 12 late	
3B Load	1 cycle ~20, then 50 dominant	Small 200 early, 50 dominant	
Hi Z	150	170	
Lo Z	74 dominant	150 dominant mixed with ~80	
Cable	150 and 53	170-200 with 50	
Measurement Point	Hardwire Arc 1	Hardwire Arc 2	Hardwire Arc 7
PCI Gnd	Small 44 early, some 6.7, ~1 late	Tiny 50 early, 1.3 late	Early 43 dominant, 1.3-1.4 late
Upper Array	50 dominant on late L.F.	Early 40, 0.7 and 1.4 mixed late	43 early, then 39, small L.F. late
4B Load	47-50	34-38	44
3B Load	47	33-35	42
Hi Z	53 and H.F.	50 early, 25 late H.F. on all	25
Lo Z	47	38	40-50 early, 27 late
Cable	48	40	41-44
Measurement Point	Hardwire Arc 3	Hardwire Arc 8	Hardwire Arc 9 (S)
PCI Gnd	~1	0.83	Small 40, 0.71 dominant
Upper Array	1.1	0.63	44 early, 0.67 late
4B Load	44	48 early, 40 late	40-44

**Table 7. Frequencies in MHz Observed in SCATSAT Measurements (continued)**

Measurement Point	Hardware Arr. 3	Hardware Arr. 8	Hardware Arr. 9 (S)
3B Load	Early 57 or dominant 26	46 early, 41 late	44
H. Z	56	56 with H.F. hast	25, 56 and 196
Lo Z	47	56	42
Cable	56	48	43

Measurement Point	Hardware Arr. 5	Hardware Arr. 6	Hardware Arr. 11	Hardware Arr. 12
Pull Gnd	~56 early or 11.3 late	56 early, 11.3 late	46 early, 11.3 late	43 early, 11.2 late
Upper Array	Early ~56, late ~67	53 early, 11.1 late	46 early, 11.3 late	45 early, 11.3 late
4B Load	46-45	51	43	44
3B Load	41-43	53	43-46	44
H. Z	~56 with H.F. hast	46 late	56 and H.F.	56
Lo Z	Early 131 or 46 dominant	56	56	47
Cable	56 early, 43 late	48	48-56	46

Measurement Point	Hardware Arr. 4
Pull Gnd	Early 56-86, then 22, all on 11.2
Upper Array	Early ~75 and ~26 with small H.F.
4B Load	56 early, ~26 dominant late, 100 on all
3B Load	26 with some higher freq.
H. Z	100 dominant
Lo Z	43 with H.F.
Cable	43-46

Normalization of the CDI results is quite straightforward. For all but drive point 4, the standard deviation of all drive currents was only 4.8% of the 838 mA mean value. Most of this small deviation was the result of small peak amplitude changes in going from one drive point to another. For a given drive point, the variation was even smaller. The exception was drive point 4 which had a lower drive pulse of 300 mA because of the larger damping resistor. But again, the drive level was very constant. As a result, the SCATSAT responses were constant also, and the normalization consisted merely of dividing each peak value by the mean drive current at that particular drive point.

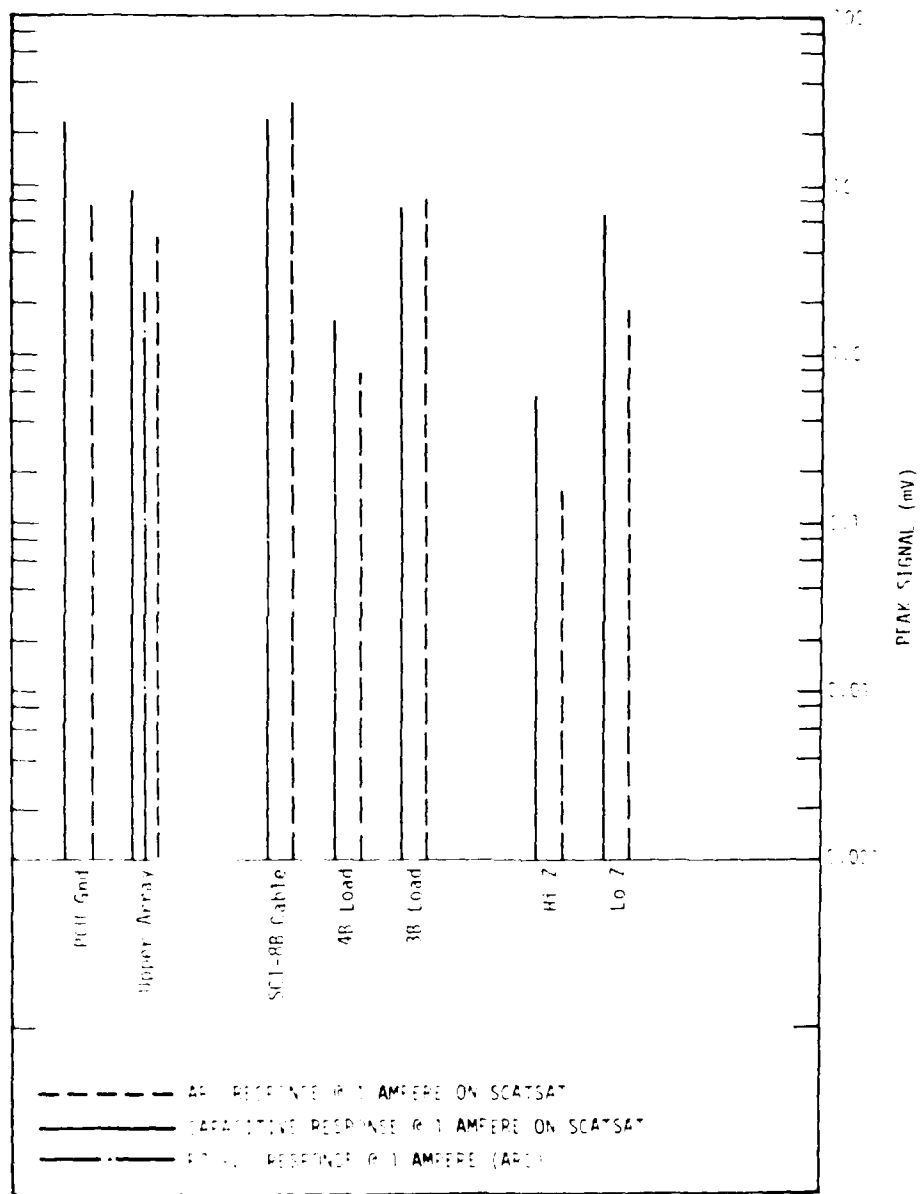


Figure 28. Comparison of arc and capacitive responses at drive point 1 for a one ampere drive current

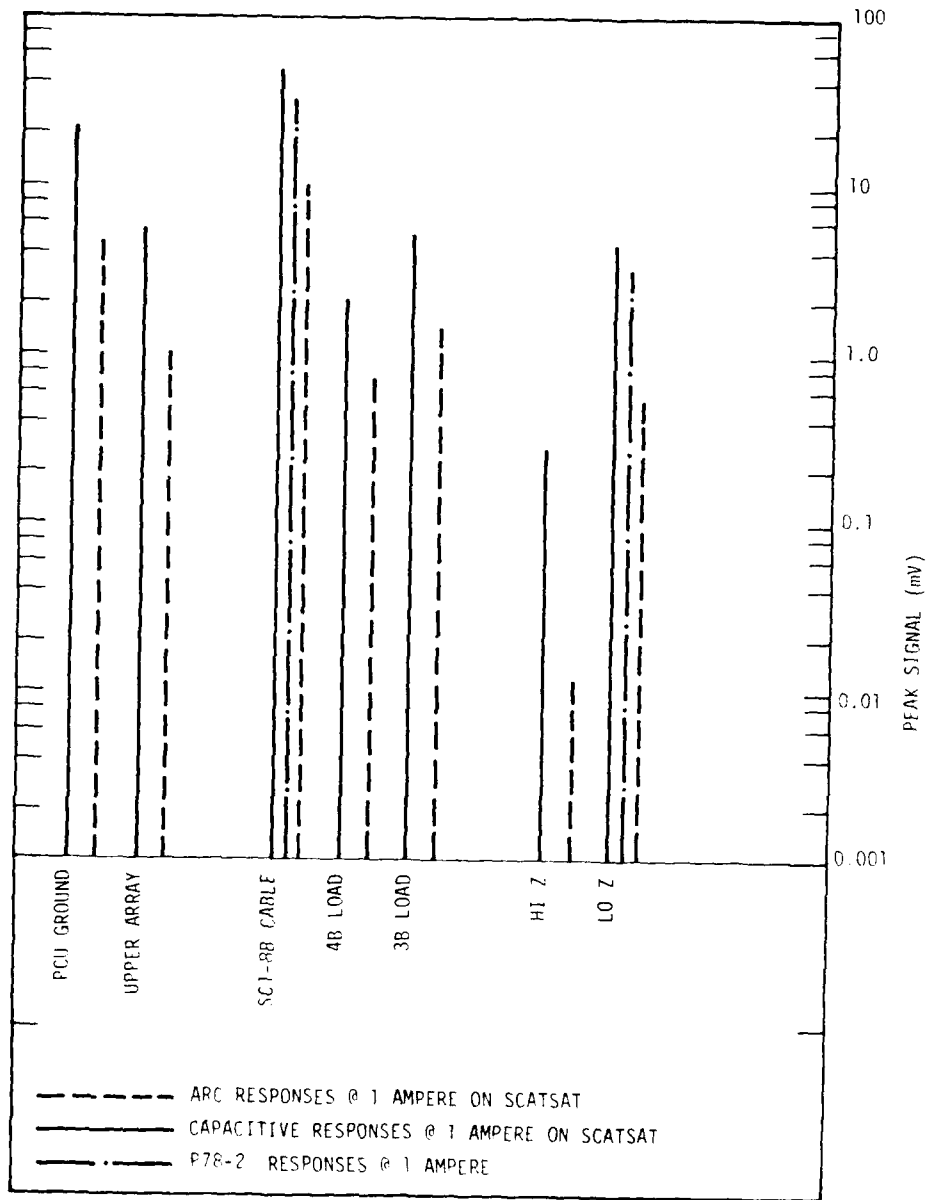
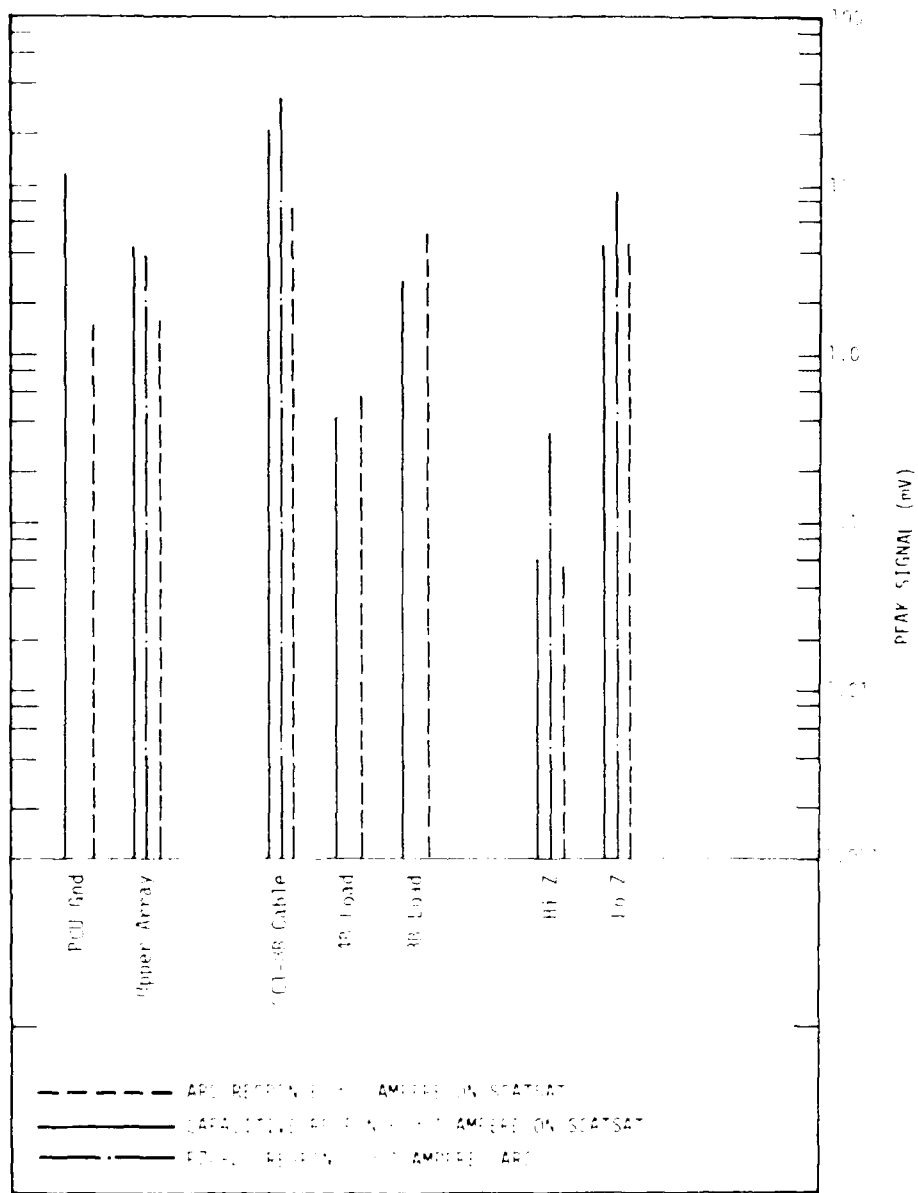
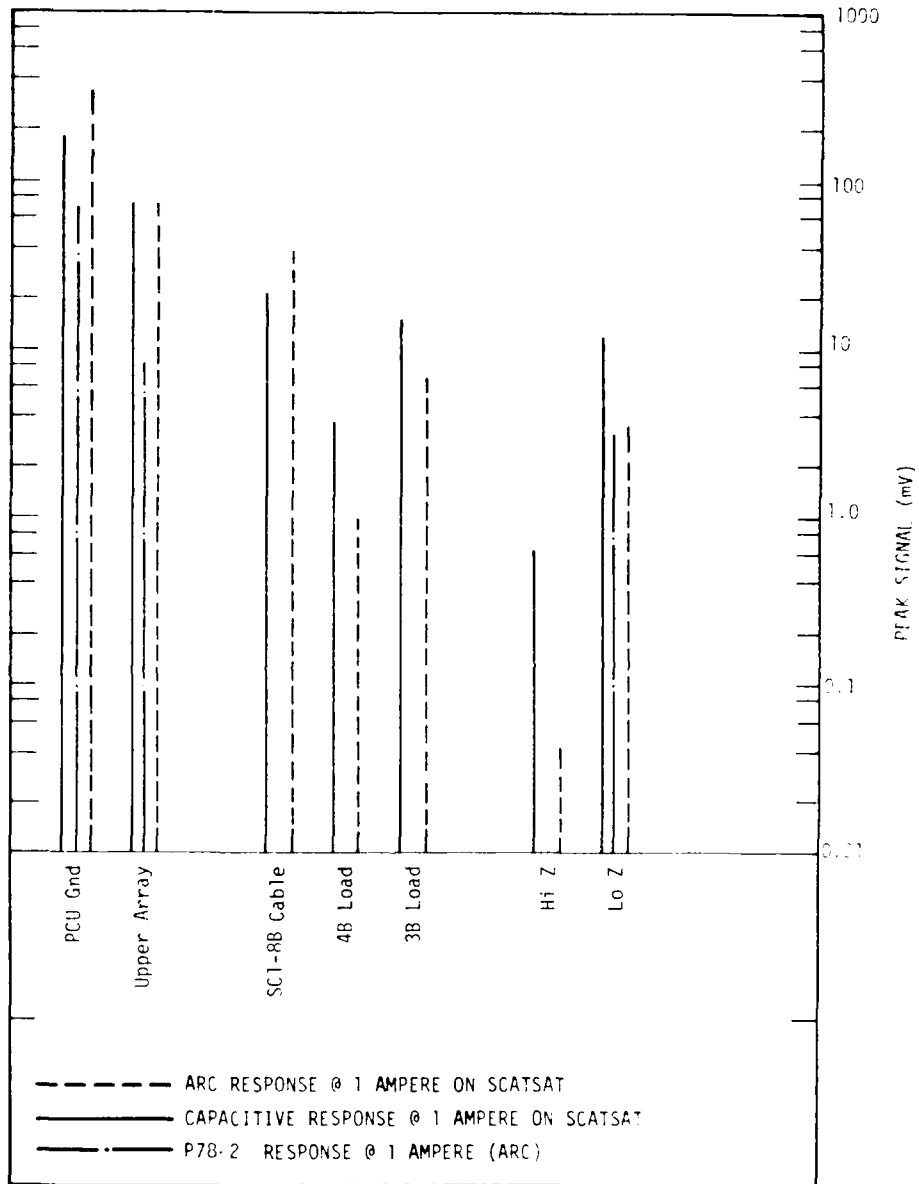


Figure 29. Comparison of arc and capacitive responses at drive point 2 for a one ampere drive current



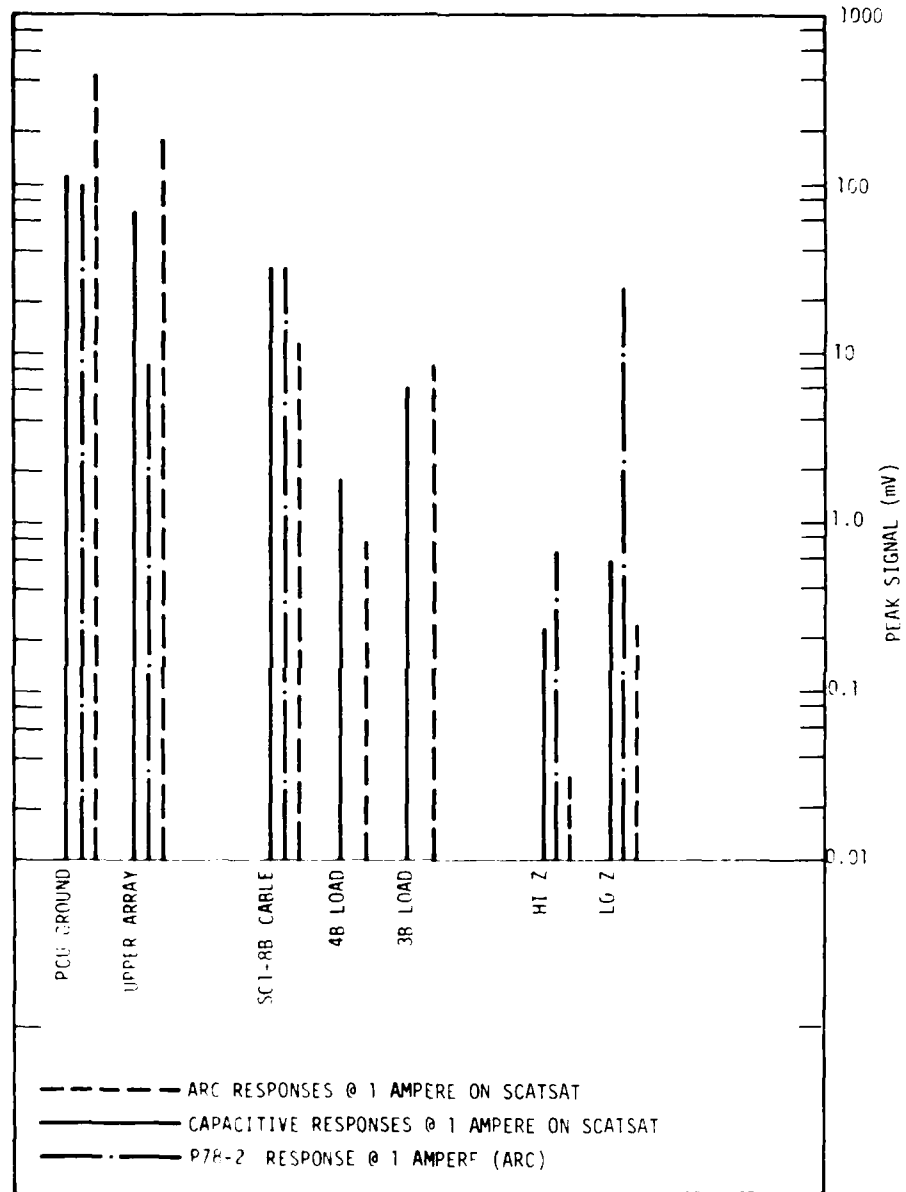
PT-1749

Figure 30. Comparison of arc and capacitive responses at drive point 7 for a one ampere drive current



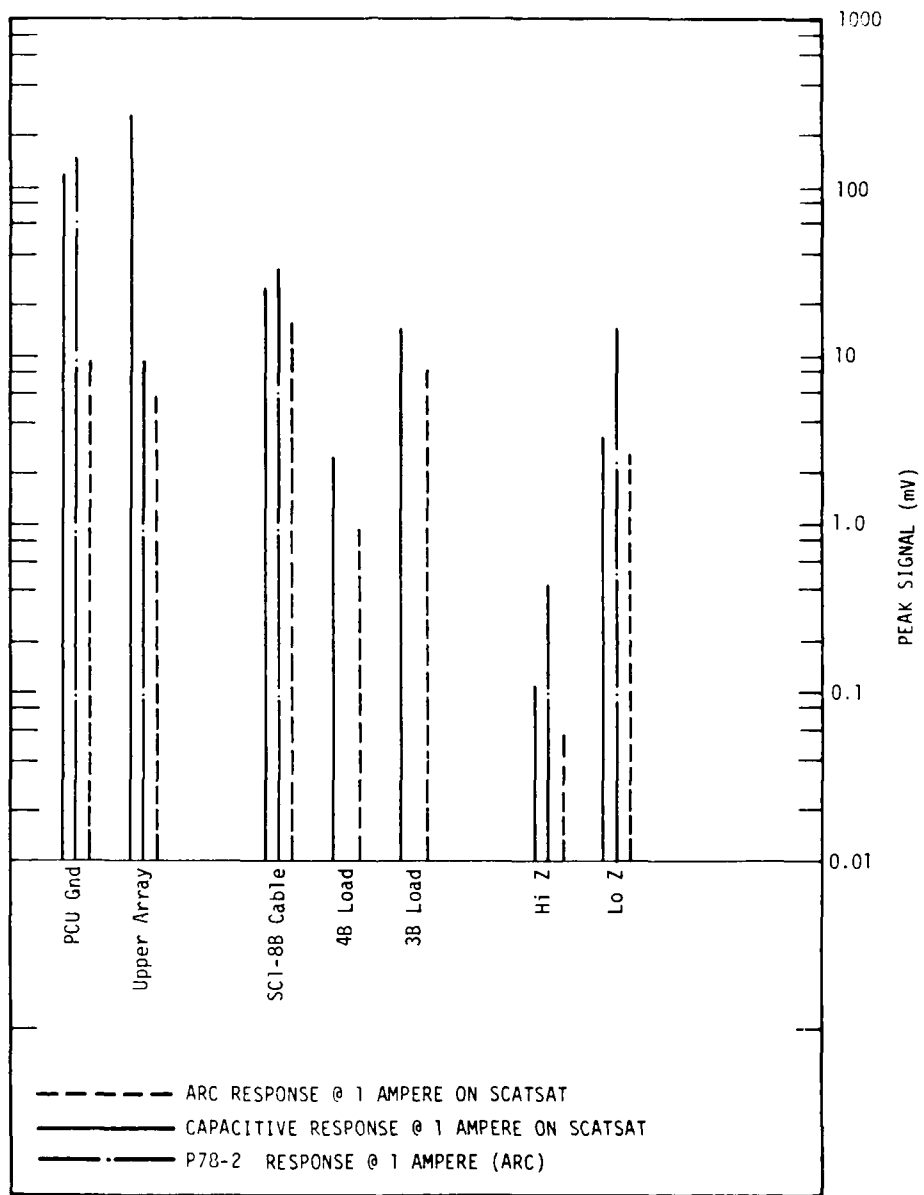
RT-17499A

Figure 31. Comparison of arc and capacitive responses at drive point 3 for a one ampere drive current



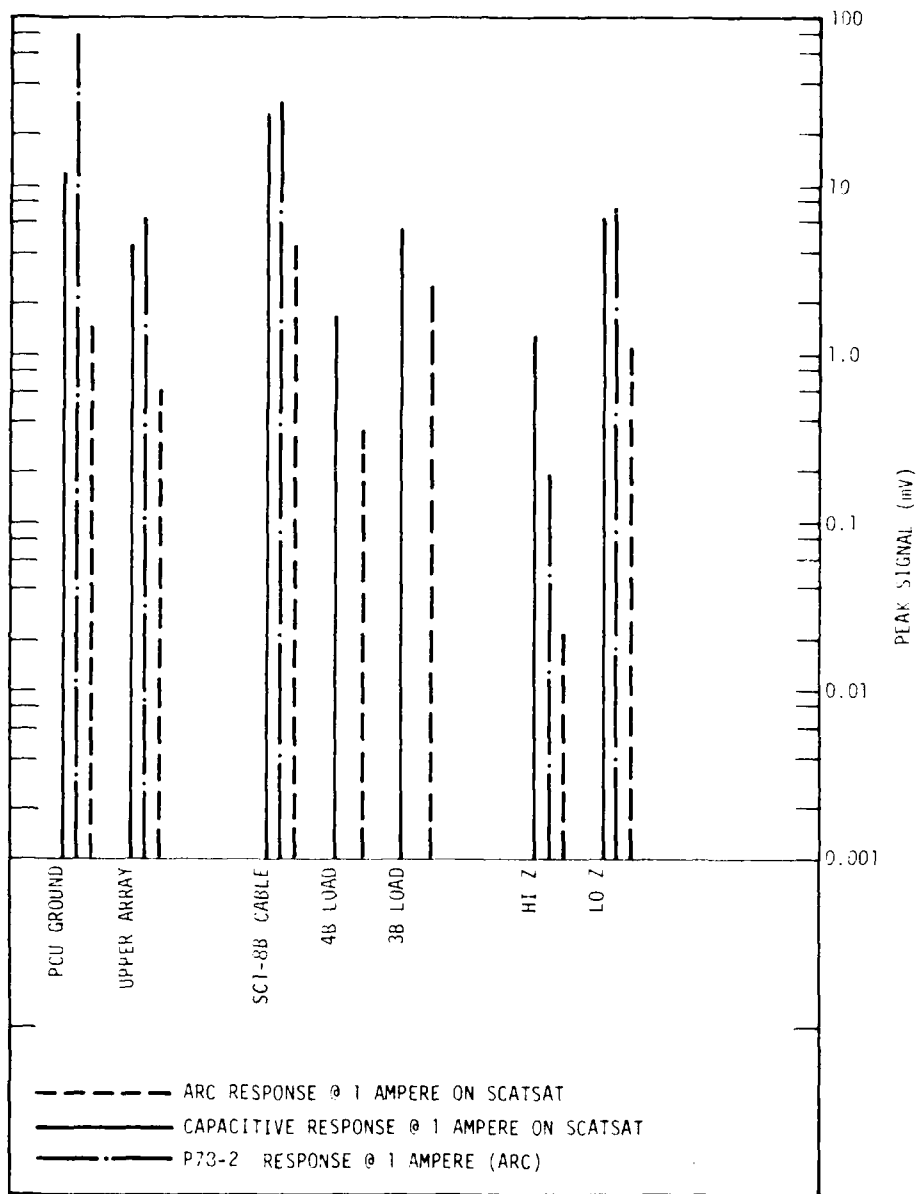
RT-17325 A

Figure 32. Comparison of arc and capacitive responses at drive point 8 for a one ampere drive current



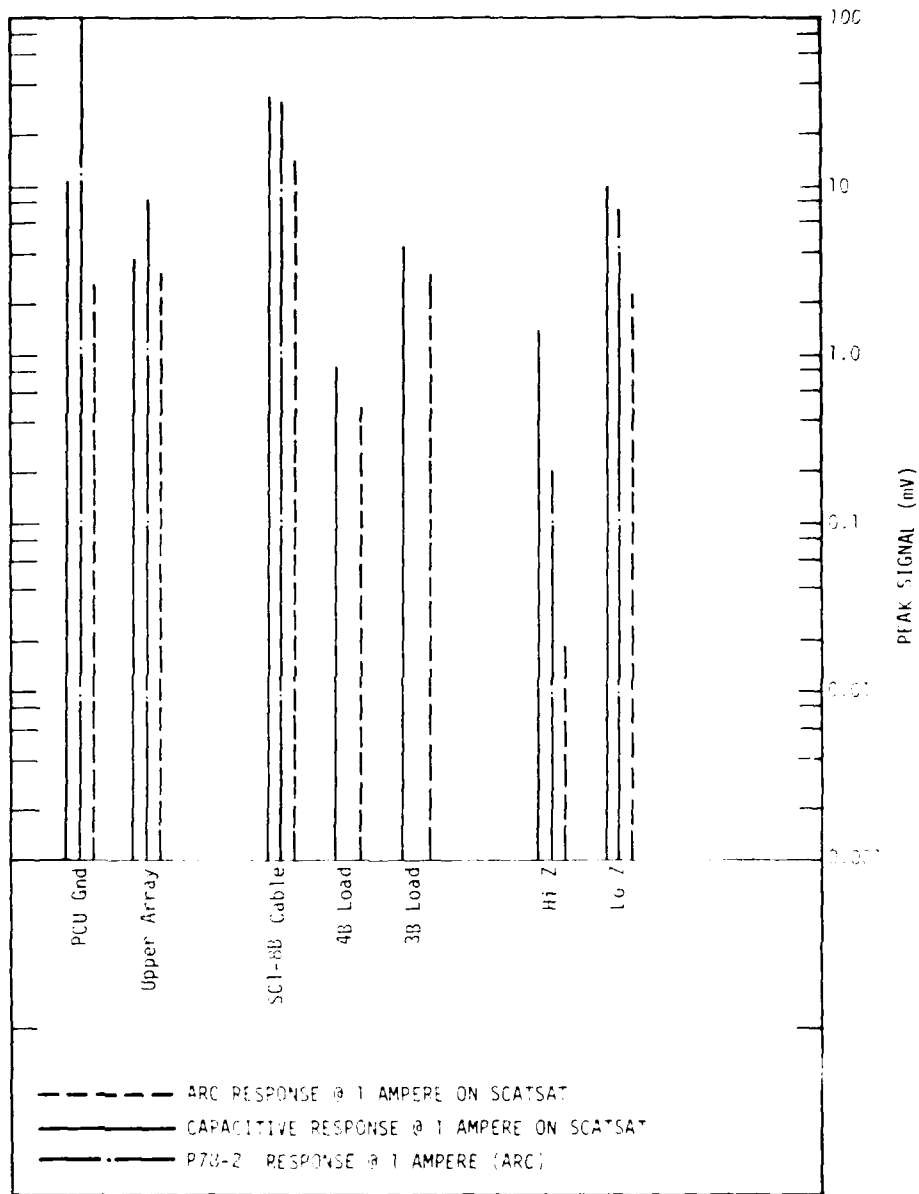
RT-17501A

Figure 33. Comparison of arc and capacitive responses at drive point 9 for a one ampere drive current



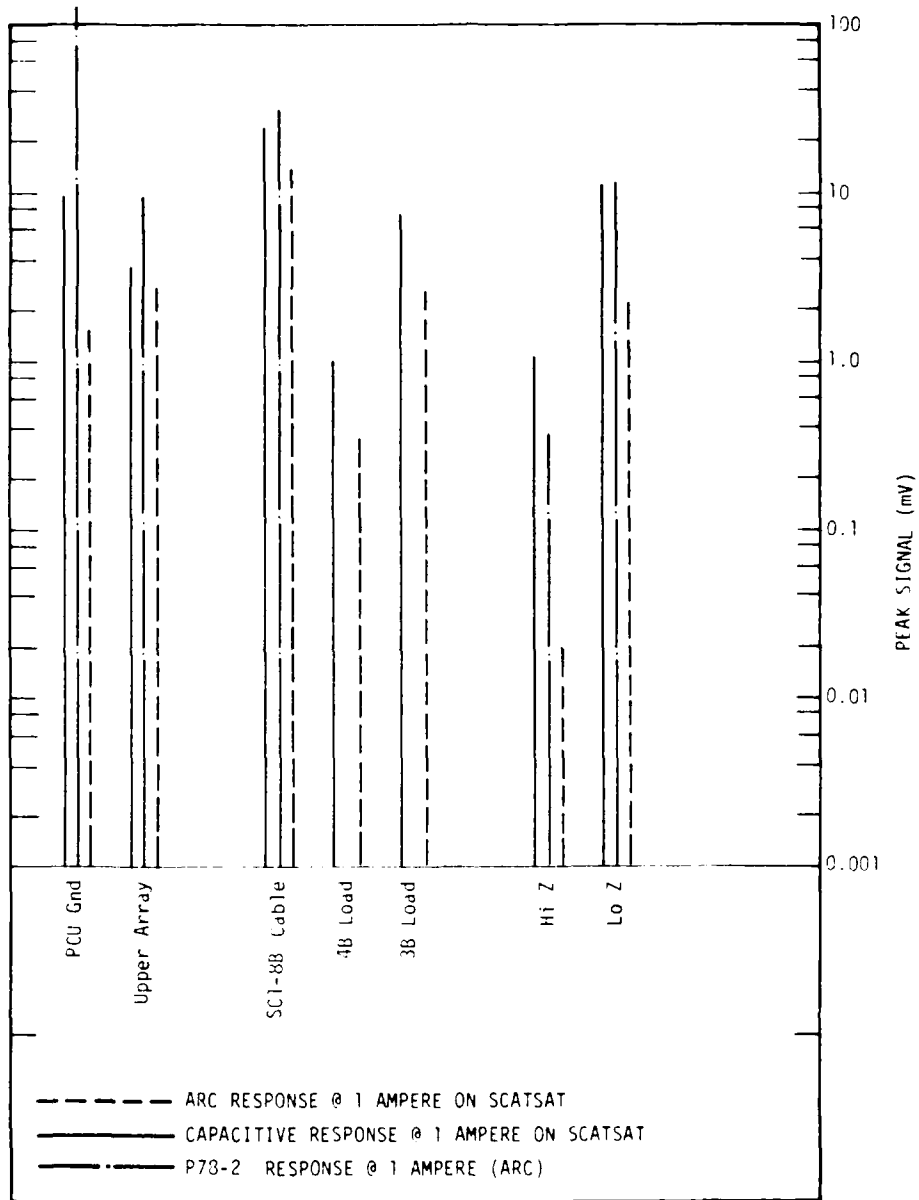
RT-17327

**Figure 34. Comparison of arc and capacitive responses at drive point 5 for a one ampere drive current**



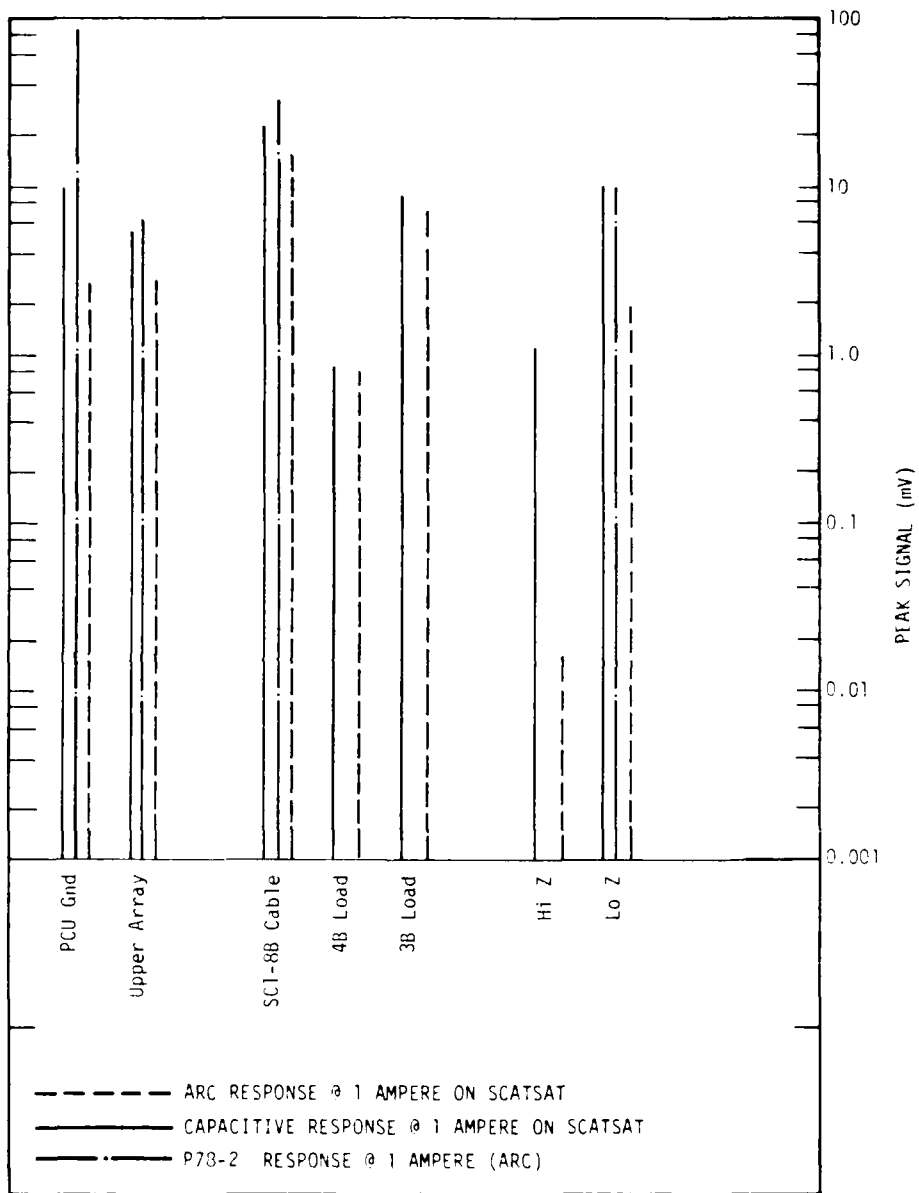
RT-17500

Figure 35. Comparison of arc and capacitive responses at drive point 6 for a one ampere drive current



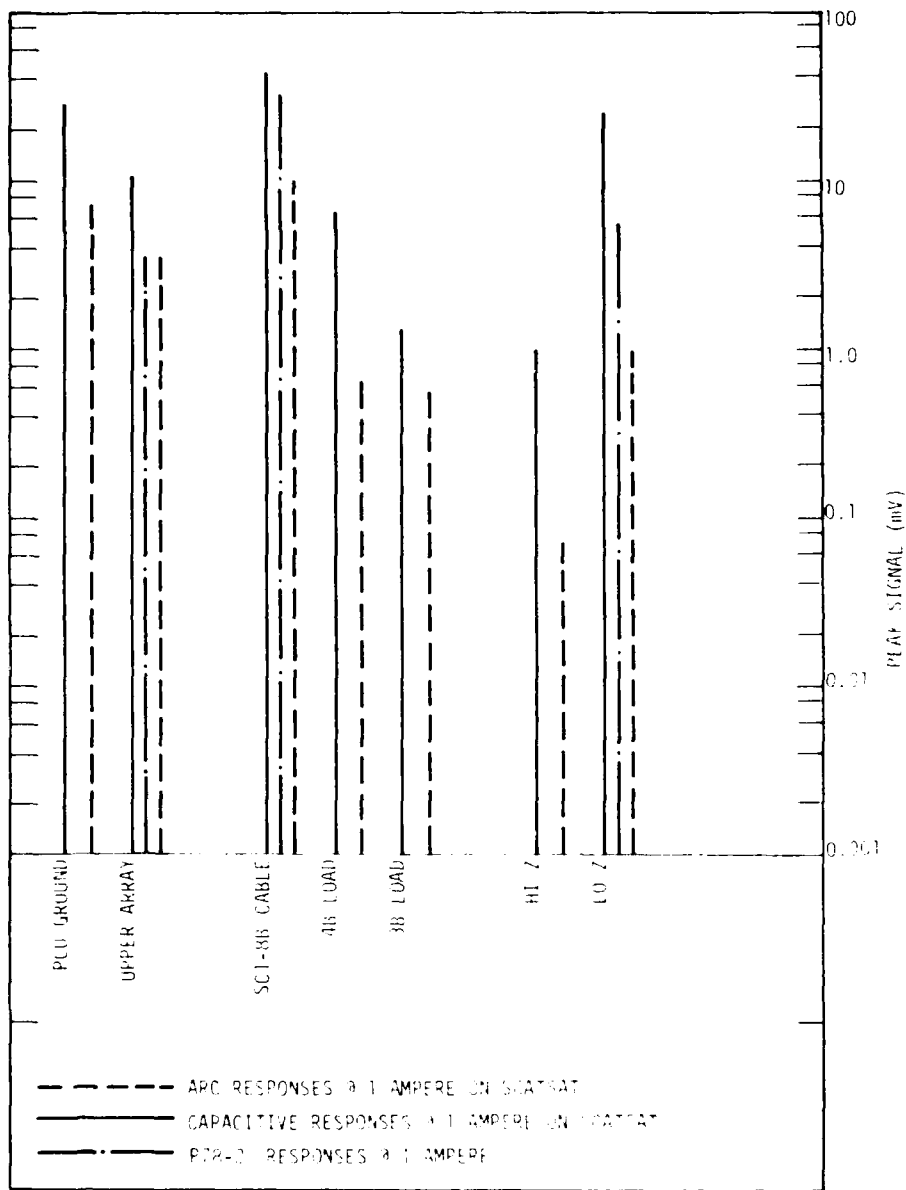
RT-17502

Figure 36. Comparison of arc and capacitive responses at drive point 10 for a one ampere drive current



RT-17503

Figure 37. Comparison of arc and capacitive responses at drive point 11 for a one ampere drive current



PT-11226

Figure 38. Comparison of arc and capacitive responses at drive point 4 for a one ampere drive current

Normalization and indeed determination of the response amplitudes for the arc injection was complicated by a much larger variation in drive current. The arc pulse waveform was characterized for a total of 57 pulses measured at intervals over the duration of the arc injection tests. The standard deviation was 27% of the 17.6 ampere average value, with a total range of as small as 7 amperes to as large as 28 amperes, a four to one range. Since the responses vary linearly with the drive current, they also varied rather widely. To obtain meaningful response data, at least three and as many as five responses were recorded at every point during the arc tests. These were then averaged to obtain the mean response amplitude. Each mean response was then divided by the mean drive current of 17.6 amperes to obtain the normalized response at one ampere. These values are plotted in Figures 28 through 38.

## COMPARISONS

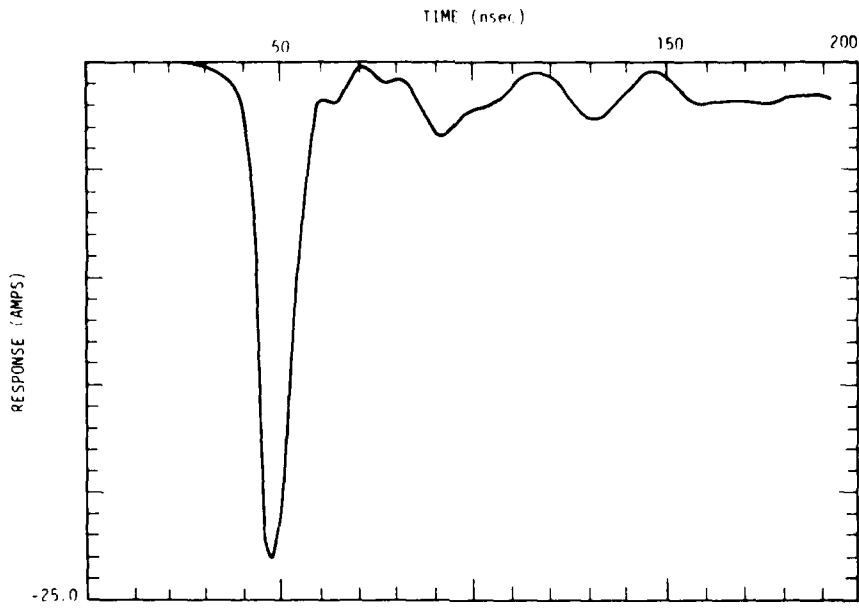
Comparisons of frequency content and normalized peak amplitudes will be made before proceeding to calculating the estimated CDI response of the P78-2.

The frequency content of arc and CDI responses may vary due to:

1. Different frequency content of the drive pulses.
2. Different ratio(s) of POE excitation, i.e., CDI may preferentially excite one or more POE's while arc injection excites other(s). The different POE's may have different characteristic frequencies.

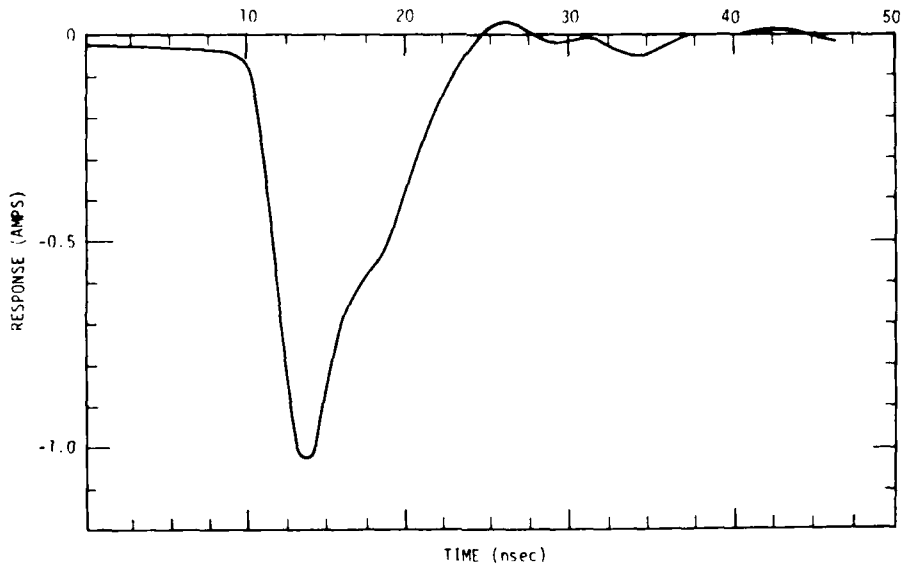
Examination of Table 7 shows that there are generally higher frequencies (>100 MHz) accompanying lower, dominant frequencies in the SCATSAT CDI responses. These higher frequencies are generally absent from the arc injection responses which otherwise have similar dominant lower frequencies. Examination of the response photos also shows that the CDI responses are nearly all more complex and "hashy" looking than the corresponding arc responses. This general trend may be due to the first reason, which prompted investigation into the drive waveforms.

The most representative drive waveforms were blown up, digitized, and Fourier transformed. The drive waveforms are plotted in Figures 39 and 40 and their transforms in Figures 41 and 42. The interesting comparison is the relative frequency content in the 100-200 MHz region to that at around 50 MHz where many of the dominant response frequencies occur. This is shown in Table 8 for four average frequencies appearing in the CDI responses. As suggested by the responses and expected from the faster risetime of the CDI drive current, it has a much larger high



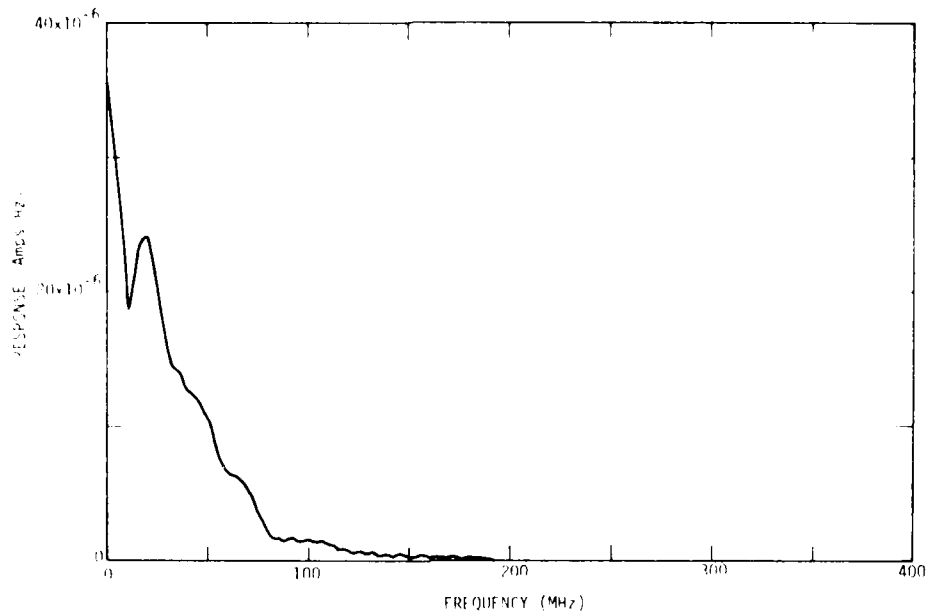
RT-17496

Figure 39. Arc current



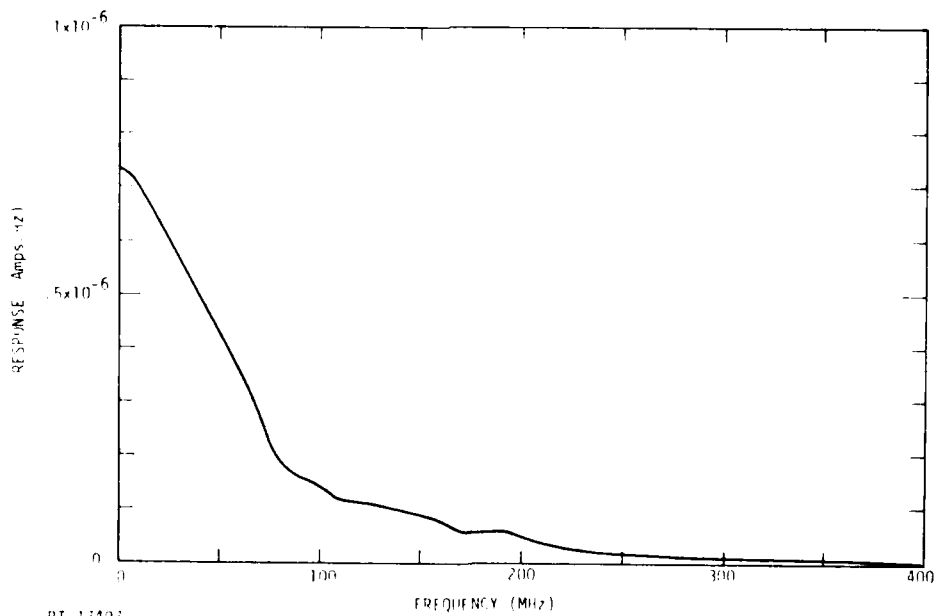
RT-17494

Figure 40. CDI current



PT-17495

Figure 41. Fast Fourier Transform of arc current



PT-17497

Figure 42. Fast Fourier Transform of CDI current

frequency content relative to 50 MHz than does the arc drive current. This accounts at least partially for the lack of high frequency in the arc responses.

**Table 8. Comparison of High to Mid Frequency Content for CDI and Arc Currents**

Frequency MHz	CDI A/(0.4MSEC)	Arc A/(0.4MSEC)
135	0.25	0.06
150	0.21	0.03
175	0.13	0.02
200	0.11	0.01

The effect of the second of the possible reasons for differing frequency content is much more difficult to assess. In Reference 7 we concluded that CDI resulted in much larger body surface current at a significant distance from the drive point than was the case for arc injection. This wider spread response may excite additional points of entry not excited by the arc injection, especially POE's sensitive to the generally higher frequencies associated with external body resonances. Differences in frequency content at specific drive or measurement locations may be due to this effect, but unfortunately are masked by the general trend to higher frequency content of CDI. However, there are some specific examples of this effect at lower frequencies. A mid frequency (5-15 MHz) appears in some of the solar array associated measurements for CDI which are absent in the arc responses. Similarly in the 4B load measurement, some CDI responses had a component around 10 MHz which doesn't appear in the arc responses. Yet the transforms of both pulses are about equally rich in 10 MHz as compared to 50 MHz. Thus, one must conclude that an additional POE is being excited by the CDI.

Because of this latter effect, there is actually no reason to expect exactly equal frequency content in the responses even if the drive waveforms were identical, which they are not. But it is clear that resonances below about a 100 MHz are being excited by both drive techniques, as agreement of frequency content in this region is generally good. These findings are evidence of the fact that the response produced depends not only in the detailed nature of the excitation, i.e. pulse amplitude and frequency, but also on the manner in which it is applied, i.e. how and where applied. Moreover what constitutes the worst case response depends not only on the threat but on the detailed construction of the object stressed.

Very little can be said about frequency content of the P78-2 experiment vs that observed in the SCATSAT experiment. Four of the five P78-2 measurement points

record only peak amplitude data. The only "time history" data comes from the SC1-8B experiment which sampled the harness wire signal, "Cable," at logarithmically spaced time intervals. But even here, reconstruction of the signal waveform is difficult since nothing is known about exactly where on the waveform the threshold (zero time) occurs, the sample window time (which of necessity is finite), etc.

It can be stated that some of the data available for this measurement on the P78-2 are not inconsistent with observations from the SCATSAT experiment. That is, the measured SCATSAT dominant frequency for this measurement ranged from 43 to 50 MHz. Scaling for P78-2 to SCATSAT size means that the dominant frequency on P78-2 should be in the range  $31 \pm 3$  MHz and it appears possible to fit a sinewave of this frequency to the reported data samples. Also, the envelope of SCATSAT data is consistent at least with the reported P78-2 data for arc location 8. Here the largest measured value occurred at 100 ns and significant signals still existed at  $>200$  ns. The SCATSAT data for drive point 8, both CDI and arc injection, show the signal also peaking at 100-150 ns and ringing to  $>200$  ns. Unfortunately, the SCATSAT cable response for most other injection points also showed ringing to  $>200$  ns while the P78-2 data do not. Without knowing the amplitude resolution of the SC1-8B, it is not possible to determine whether or not it is possible for it to have missed these later signals. Certainly there is not a warm feeling about the agreement for arc points 1 through 7. SC1-8B measured nothing as early as 7 ns after the threshold was crossed while all the SCATSAT data rang well beyond this time.

Comparisons of normalized peak response amplitudes have been made for CDI vs arc injection on the SCATSAT and for arc injection of SCATSAT vs arc injection of P78-2. The former are of interest in determining whether an object of satellite like complexity exhibits the same larger responses for CDI simulation of outward charge emission as the surface currents on the simple body (Ref. 3). The latter are of interest in determining how faithful a representation of the P78-2 has been achieved in the SCATSAT.

The comparisons can be made in a couple of different ways. One is to plot data for each injection point with measurement location as the variable. This has been the form of presentation of the data so far. The other method is to plot all data for each measurement location with injection point as the variable.

The second technique is useful for identifying patterns of response amplitude as a function of where the object is driven. Such a pattern shows up strongly in Figures 43 and 44 for SCATSAT CDI drive. Here the solar array associated measurements, PCU

ground and upper array, show much greater response when the solar array was driven at points 3, 8, and 9. The same pattern does not appear in the P78-2 data. As a consequence, when the arc injections of SCATSAT were made, we made some modifications to see if we could duplicate the P78-2 results, as well as duplicating exactly the previous CDI drives. In Figures 45 and 46, data are plotted for arc injections directly to the solar array at points 3 and 8 as was done in the CDI, but point 9 was injected to the array substrate instead of the array itself. Data was also taken (but not shown) for arc injection to 0.008 inch fused silica cover glasses over the simulated array at points 3 and 8, to see if this had an effect on the pattern. Figures 45 and 46 shown that when the array was driven directly by the arc, it had the same strong coupling to PCU ground and upper array that CDI did. Even when the cover glasses were added, the pattern did not change but the level of all measurements merely shifted downward by a factor of about 3 to 5. Only when the substrate was driven rather than the array itself did the response behave as did the P78-2. We conclude from this that either (1) our simulation of the solar array penetration is very poor or (2) the P78-2 arcs were also to the substrate rather than being directly to the solar array or cover glasses. The first reason seems unlikely since we have simulated this major penetration very faithfully.

The data plots using the second technique show no other significant patterns than those associated with injection directly to the solar array. The P78-2 data is generally rather flat with the Low Z antenna showing the greatest range. The SCATSAT data shows generally wider ranges of data distribution especially for arc injection, but still no pattern.

The data were plotted in Figures 28 through 38 so that all the SCATSAT and P78-2 responses for a single drive point can be compared easily. Ignoring drive points 3 and 8, which will be discussed separately, two strong patterns appear in these comparisons. First, in 57 of 63 measurements CDI produced greater responses than did arc injection. Four of the six where this did not occur were associated with drive point 7 and the other two occurred at drive point 1. Both of these are on the central structure around the belly band, specifically to boom mounting brackets. The CDI responses were greater than arc responses by a factor of about two to almost two orders of magnitude. Second, for 33 of 34 measurements the P78-2 response to arc injection is greater than the SCATSAT response to arc injection. The one place where this did not occur was again at drive point 1 on the central structure. This suggests that the SCATSAT was not as leaky as the P78-2, especially in the region of the central

structure. This is not too surprising since this is probably the area on the model where greatest "experimental" (i.e., P78-2 experiment) complexity was left out of SCATSAT. There are many penetrations in this region on the P78-2 which should be simulated for further testing.

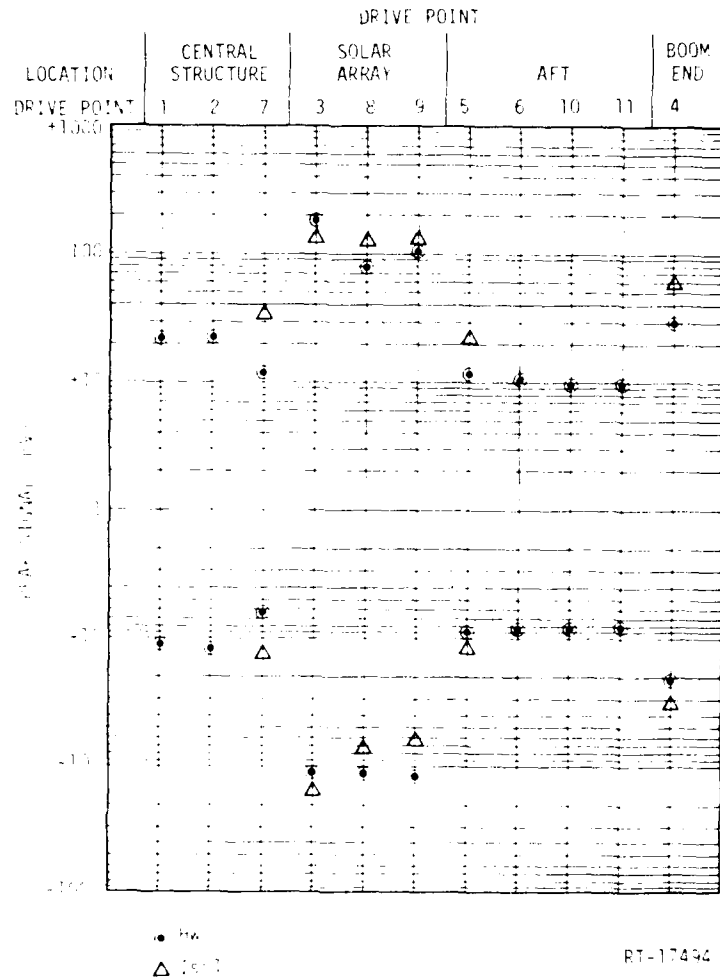


**Figure 43. Peak signal observed on "PCU Ground" for capacitive direct injection at the eleven drive points. Data normalized to one ampere drive.**

The responses at drive points 3 and 8 behave differently because of injection directly to the solar array as previously discussed. The PCU Ground and Upper Array measurement points on SCATSAT show greater response for arc injection than for CDI.

Cross coupling between the array POE and two other cable measurements cause these to also be affected by the large currents on the array. Also because of the direct array drive, the PCU Ground and Upper Array responses to arcs on SCATSAT are greater than the same measurements on the P78-2. These SCATSAT responses are considered non-representative of the P78-2 arc tests because of the apparent difference in exact injection point.

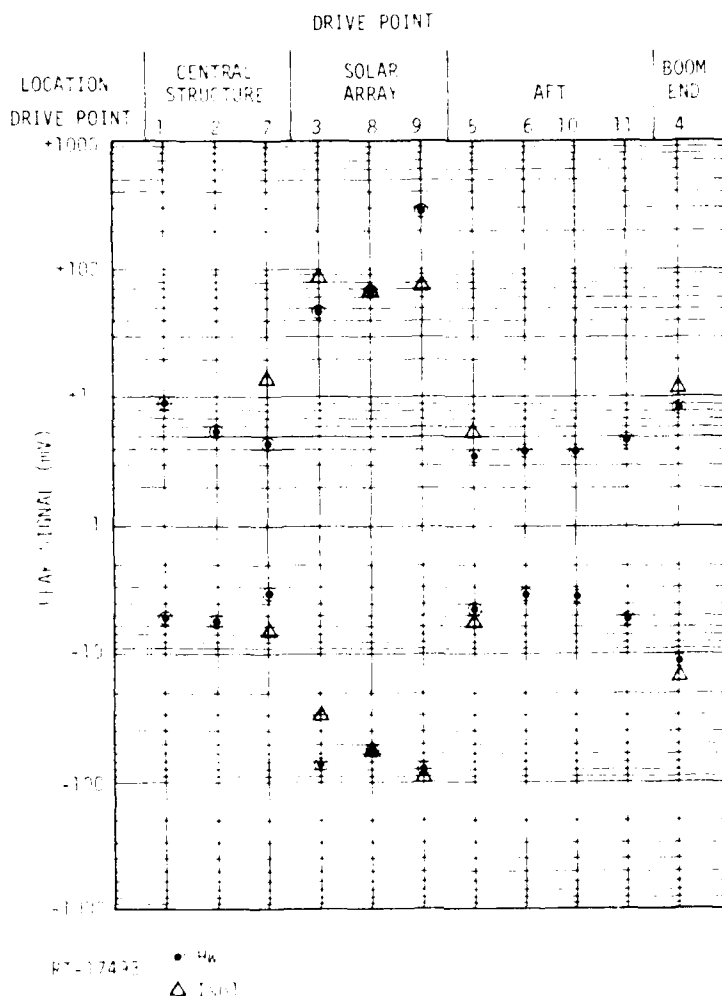
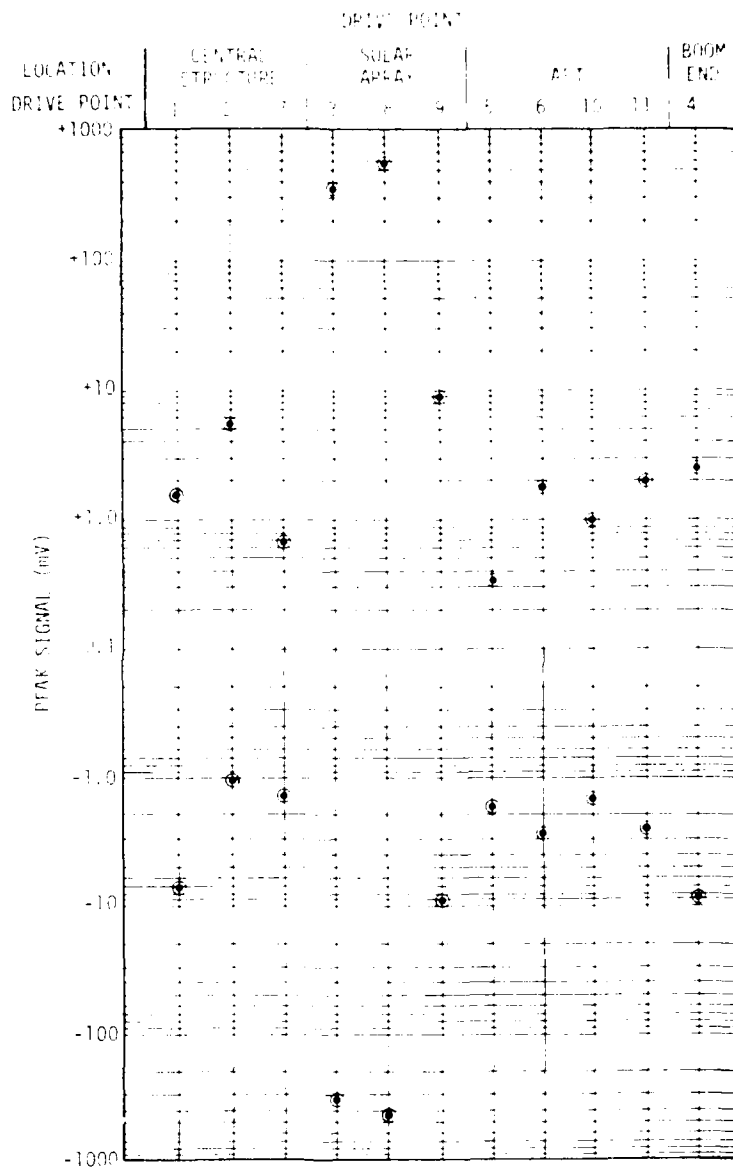
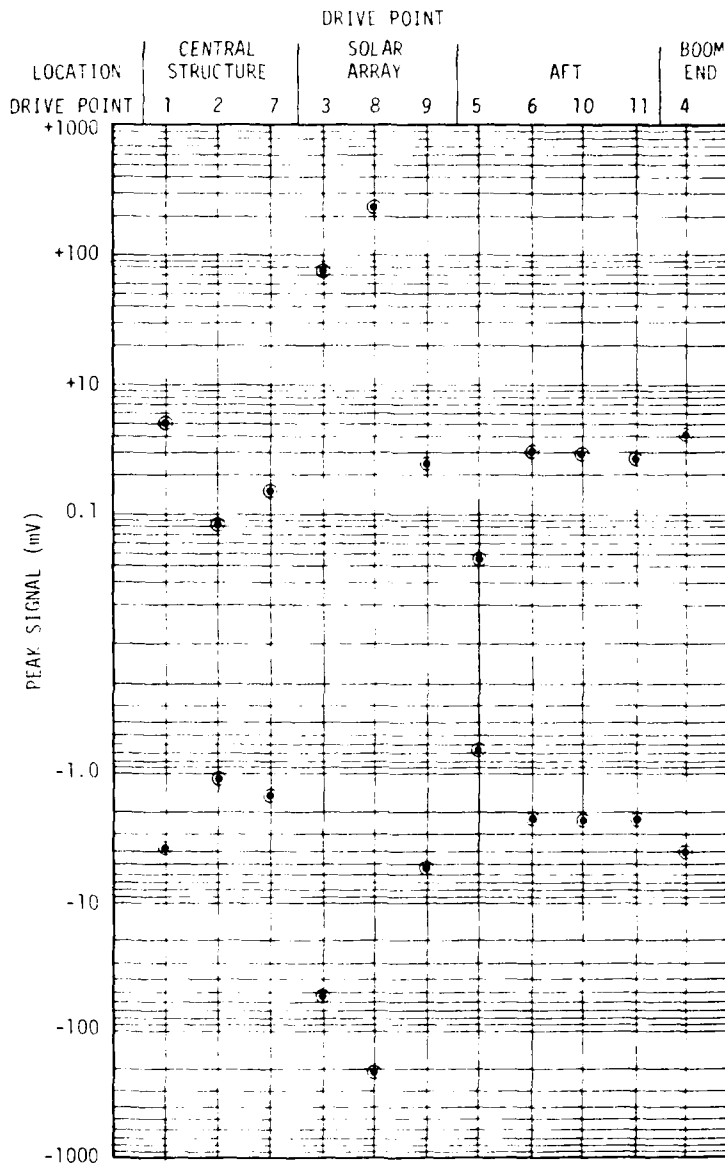


Figure 44. Peak signal observed on "Upper Array" for capacitive direct injection at the eleven drive points. Data normalized to one ampere drive



RT-17491

Figure 45. Peak signal observed on "PCU Ground" for arc injection at the eleven drive points. Data normalized to one ampere drive.



RT-17492

**Figure 46.** Peak signal observed on "PCU Ground" for arc injection at the eleven drive points. Data normalized to one ampere drive.

In taking and analyzing the SCATSAT data, a distinct pattern emerged as far as the relative amplitude of several of the measurements points on the model were concerned. In order of largest to smallest, the order was:

- SCI-8B Cable (all)
- PCU Ground (all)
- Upper Array, Low Z, 3B (mixed and nearly equal)
- 4B (9 of 11)
- High Z (all)

The P78-2 responses also exhibit an order as follows:

- PCU Ground (all)
  - SCI-8B Cable (all)
  - Low Z
  - Upper Array
  - High Z (all)
- } Sometimes equal

Except for the reversal of PCU Ground and Cable, the relative response pattern on the SCATSAT model was quite similar to the P78-2 for the five P78-2 responses reported.

## CALCULATION RESULTS

One of the purposes of this effort was to make estimates of the P78-2 response to a CDI simulation of charge blowoff, based on the experimental results. The calculations to do this and the results are presented in this section.

An important note of caution is in order before preceeding, however. Despite significant efforts to duplicate the electromagnetic characteristics of the P78-2 in the SCATSAT, it is still not the P78-2. The resulting SCATSAT responses are similar to the P78-2 responses but not duplicates. Therefore the results of the following calculations are indicators of how the P78-2 may respond rather than firm predictions. More must be known about the coupling paths before predictions are possible. This can only be determined from a more detailed coupling and susceptibility analysis.

The parameters of interest are the margins for upset of critical circuits in the P78-2. Twelve critical circuits have been identified and their thresholds determined. The circuit thresholds are twice the "set thresholds" used in conducted interference tests of Reference 2. The cables which connect to the least and most sensitive of these critical circuits are simulated in SCATSAT by "3B Load" and "4B Load" respectively.

The measured responses on these lines were scaled to their estimated P78-2 response level for CDI and compared to the upset thresholds. The scaling is based on the experimental results which show (1) the P78-2 to be more leaky than SCATSAT and (2) that CDI generally produces greater response than arc injections.

The simulated critical circuits are located in the main cable bundle where the "Cable" measurement point for SC1-8B is also located. Therefore it is reasonable to examine the variation of "Cable" response for the P78-2 vs SCATSAT, and capacitance vs arc injection of SCATSAT, to draw some conclusion about how large actual signals on these points might be when arcs occur in space. The measured 4B load (Critical Circuit 12) and 3B load (Critical Circuits 9 and 10) have been scaled to one ampere of outward emission current from the P78-2 by the following equation.

$$P78-2 V_{L(CDI)} = SCATSAT V_{L(CDI)} \times \frac{P78-2 V_C (Arc)}{SCATSAT V_C (Arc)}$$

where  $V_L$  = Load voltage on 3B (CC 9/10) or 4B (CC 12), measured on SCATSAT and estimated for the P78-2.

$V_C$  = Measured "Cable" response

The ratio is, of course, the measure of just how much more energy is coupled into the P78-2 for a particular injection point than into the SCATSAT. Again a note of caution is in order. The "Cable" results from the P78-2 arc tests are totally flat at 1.27 volts, the threshold of the experiment for all injection points. The SCATSAT results for this particular measurement were also relatively flat, but did show variation of about a factor of three from minimum to maximum as different points were injected. Thus, one might ask whether the actual peak "Cable" signal varied also and simply failed to show up because of the constant experiment threshold. This would have some impact on the results of these calculations, which are shown in Table 9. The outward emission current which will raise the signal on these lines to the critical circuit threshold is also shown in Table 9. This is calculated by dividing the threshold voltage by the estimated load voltage per ampere. The circuit 12 threshold is 170 mV and the circuit 9/10 threshold is 11,000 mV.

Clearly, the lowest upset threshold is for circuit 12, with 2 to 30 amperes of outward emission current required. The emission charge has been estimated from the literature to be about  $2 \times 10^{-7}$  coul/cm<sup>2</sup> (Ref. 6). For a current waveform which is

similar to the experimental waveforms and 10 ns wide, the areas required to discharge are in the range of 10 to 150 cm<sup>2</sup>. There are many dielectrics on the P78-2 of much larger area than these, therefore it appears likely that some critical circuit upsets may appear when the P78-2 is on orbit.

**Table 9. Estimated P78-2 Critical Circuit Responses**

Critical Circuit	Signal Voltage per Amp Emitted (mv/amp)				Threshold Emission Current (amps)			
	Point 2	Point 4	Point 5	Point 8	Point 2	Point 4	Point 5	Point 8
12	7	20	14	6	24	7	12	30
9 and 10	15	5	6	20	730	2000	260	550
	Point 6	Point 7	Point 9	Point 10	Point 6	Point 7	Point 9	Point 10
12	58	24	88	85	2.9	7.1	1.9	2.0
9 and 10	43	18	60	89	260	610	180	120
	Point 1	Point 3	Point 11		Point 1	Point 3	Point 11	
12	No data	No data	37		No data	No data	4.7	
9 and 10	No data	No data	39		No data	No data	280	

The question naturally arises that if upsets are predicted for only 2 to 30 amps of outward emission, would they be expected for the 40 ±10 amps estimated current in the P78-2 arc tests? This can be answered by multiplying the 1 amp 4B Load (Critical Circuit 12) voltage observed in the SCATSAT arc tests by the ratio of Cable response for P78-2 arc to the Cable response for SCATSAT arc and the 40 amp P78-2 arc current. Expressed as an equation

$$P78-2 V_{L(Arc)} = SCATSAT V_{L(Arc)} \times \frac{P78-2 V_{C(Arc)}}{SCATSAT V_{C(Arc)}}$$

The results for the eleven injection points are:

Point	P78-2 CC 12 Voltage
1	<32 mV
2	90 mV
3	<33 mV
4	90 mV
5	105 mV
6	44 mV
7	116 mV
8	85 mV
9	73 mV

<u>Point</u>	<u>P78-2 CC 12 Voltage</u>
10	33 mV
11	59 mV

These estimated critical circuit 12 voltages are 19 to 68% of the threshold, so the answer is that no upset of this circuit would be expected for these eleven injection points during the arc tests. If none of the other critical circuits are connected to wires with significantly greater leakage, then no upsets would be expected at all during the P78-2 arc tests. This agrees with the results reported by MMC that "There were no anomalies as a result of the static discharge to the vehicle," Reference 10.

#### 4. SOLAR ARRAY EXCITATION

Continuing puzzlement about the differences between SCATSAT and P78 2 responses to solar array injection resulted in some important realizations about proper technique for simulating EID on solar arrays. The problem arises from the fact that the solar array is basically a string of semiconductor diodes so that (1) the polarity of injection becomes important and (2) the illumination level may be important. A schematic representation of an array including stray coupling to structure and the load circuit is shown in Figure 47. A blowoff of electrons due to EID on one of the cell cover plates is represented by the current generator. Note that the negative charge of electrons emitted from the array is the same as a positive conventional current injected onto the array. This positive current can then flow easily to the negative pickup wire through the forward biased cells and to the structure via the power single point ground (SPG). Of course, some of the injected current will also flow directly to the structure via the cell to substrate capacitance which is of the order of 10-20 pF per cell.

The cells above the arc point are reverse biased and will therefore tend to block current, especially on the shadowed side of the space vehicle. Because of this, the degree of laboratory illumination may be important to EID simulation quality. In a poorly lit area or one where the illumination spectrum is poorly matched to the cell sensitivity, these reverse biased cells will represent a higher impedance than will be the case of full illumination on orbit and a lower impedance than when shadowed on orbit. Thus, coupling to the positive pickup wires may be poorly simulated in the laboratory environment.

A negative conventional current injected at the point shown is blocked from both positive and negative pickup wires by the cells on one side and the blocking diodes on the other. This, of course, would make for a very poor simulation of EID. A very key observation here is that the injection circuit of Figure 6 in Mil-Std 1541 will produce exactly that negative current injection if the SCR end of the auto-transformer is grounded to the test object and the arc taken from the high voltage end of the secondary. It is very important that the injection be polarized to produce a positive conventional current into the array.

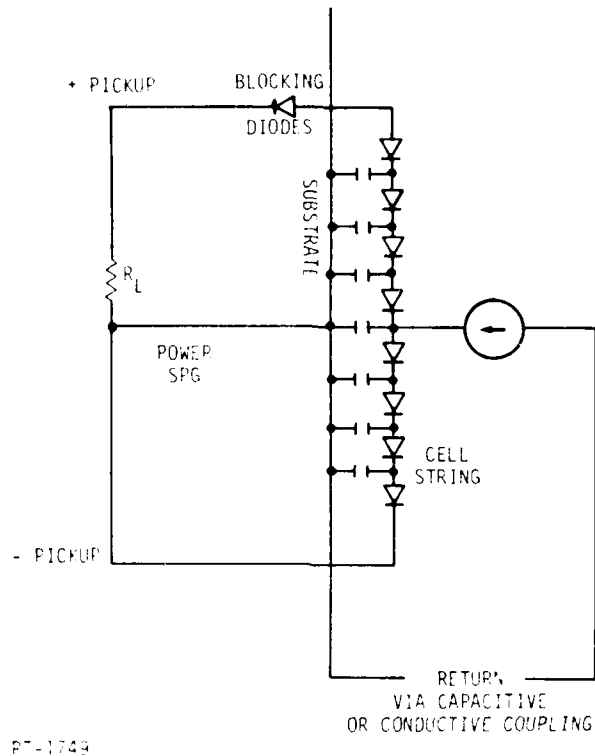


**Figure 47. Schematic of real solar array with EID injection**

The problem of injection polarity does not exist with SCATSAT since it is a completely linear model, i.e., there are no semiconductor devices such as the cells or the blocking diodes. The "solar arrays" are strips of highly conductive copper tape rather than the uncertain conductivity of the real solar cells on the P78-2, which may account for the observed difference in coupling when the array is driven. Whether the metal strips are a better or worse simulation of the actual on orbit condition is not known at this time. This area is worthy of some investigation since the array is a potentially major penetration on most satellites and its proper excitation is very important to system level EID testing.

## 5. CONCLUSIONS AND RECOMMENDATIONS

Responses of the SCATSAT model of the P78-2 space vehicle been measured for two drive techniques which represent different aspects of an electron induced discharge. Complete sets of high quality data were obtained for the five measurements and eleven drive points which parallel those used in the MMC arc tests on the actual P78-2, and for two additional measurements representing P78-2 critical circuits 9/10 and 12. The SCATSAT data were analyzed and then used to scale the measured responses of the P78-2 to what might be expected if it were driven with a capacitive direct injection simulation of charge blow off.

This effort has used a physical representation of the P78-2 rather than an analytical one to help quantify coupling effects. Such an approach has the advantage of including in a single model everything we perceive to be important to the coupling chain and in greater detail. The complexity of the real space vehicle precludes doing this in an analytical approach. The principal disadvantage of the physical model is the inability to easily vary elements to study sensitivities and thereby improve understanding of the coupling mechanisms. In either approach possibly erroneous perceptions can result in a less than perfect representation of the real system. This study has the advantage of having real system responses which we can compare to our simulated responses to see how well we are doing. The comparisons show clearly that we have not succeeded in exactly duplicating the P78-2 because the responses are not identical. The principal difference is that the relative amplitudes of the two largest responses are reversed. But it is also apparent from the comparisons that the model is a reasonable representation.

The indirectly measured P78-2 responses also seem to have been well represented. The signal levels estimated for the most sensitive P78-2 critical circuit from the SCATSAT and P78-2 data show that they are below the circuit threshold for all drive points. This indicates that no upsets should have been observed in the P78-2 arc tests and this was indeed the case.

We draw the following conclusions from the experimental data and calculations.

1. Capacitive direct injection can produce larger internal responses in a complex object, amp for amp, than does arc injection, though the differences are somewhat smaller than previously predicted for external surface current responses (Ref. 3).
2. Arc injection produces larger responses than CDI when the arc point is coupled directly to the measurement point, i.e., the solar array.
3. No upsets would be expected in the arc tests of the P78-2 based on the experimental data and this was verified by the test report.
4. Critical circuit upsets are likely due to EID resulting in charge blowoff once the P78-2 space vehicle is on orbit. Calculations show emission currents of only 2 to 30 amps are required to raise critical circuit 12 to its threshold. Even with some uncertainty allowed for a less than perfect simulation, currents of a few amperes are all that are required. The corresponding dielectric areas required to discharge are of the order of tens to hundreds of square centimeters. Dielectric surfaces of this size exist in many places on the P78-2.
5. The polarity of injection is very important when simulating EID effects on real solar arrays. The degree of illumination may also be important but this hasn't been verified yet.

The objective of the arc test on the P78-2 was to verify its invulnerability to EID effects per Mil-Std 1541 techniques. Our conclusions indicate that this objective was not fully met because the arc tests do not simulate the worst effect of EID. Therefore, we also conclude that CDI should be added to the Mil-Std 1541 tests to obtain a more realistic EID simulation. This will require some development of equipment and/or techniques in order to scale the drive current up to threat levels. An increase of the order of at least ten to a hundred from the levels of the SCATSAT tests is necessary. The military standard should also be modified to stress the importance of correct injection polarity.

The logical progression of tests and analyses, of which these electrical tests are a part, should be continued. This could proceed in several areas, the most important of which is to bring together the dielectric materials testing and the electrical testing into an electron spraying experiment on instrumented, satellite-sized test objects. A simple

cylinder should be tested first, then the SCATSAT. The results would be compared to the available arc and CDI response data on these two objects to validate the quality of the electrical simulation of EID. Then more meaningful electrical testing of satellites for EID effects can be achieved.

In parallel with these tests, the parametric sensitivity study devoted to modeling EID response begun with this program, should be completed. The aim of this effort would be to more quantitatively determine how variation in different aspects of the threat: pulse shape, amplitude, coupling, affect response. This study should be driven by an awareness of which aspects of the response are important to simulate to validate the EID survivability of systems. In particular, a simple drive technique may not be a sufficient qualification tool.

Kind

## REFERENCES

1. Martin Marietta Aerospace, P78-2 SV EMC Test Plan, TL5827002, May 1978.
2. Martin Marietta Aerospace, P78-2 SV EMC Test Procedures, SCA 3504.
3. R. E. Leadon, A. L. Weiman, and R. C. Keyser, "Electrical Simulation of Electrostatic Discharges in Dielectrics," IEEE Trans. Nucl. Sci. (to be published, Dec. 1978).
4. Aerospace IOC, "Arc Discharge Tests on SCATHA-Results," Aug 11 1978, A.L. Vampola.
5. Aerospace IOC, "SCI-8B Measurements During Space Vehicle Arc Injection Tests, Aug 14, 1978, H. C. Koons.
6. R. C. Keyser, "ESD Modeling, Testing, and Analysis for SCATHA - Phase II Test Plan (Draft)," IRT 8161-016, Sept. 29, 1978.
7. R. C. Keyser, R. E. Leadon, A. Weiman, and J. Wilkenfeld, "EID Modeling, Testing and Analysis for SCATHA," Vol. I - Phenomenology Study and Model Testing, Final Report (Draft), IRT 8161-016, Sept. 29, 1978.
8. R. O. Lewis Jr., "Viking and P78-2 Electrostatic Charging Designs and Testing," Proceedings of the Spacecraft Charging Technology Conference, AFGL-TR-0051, Feb. 24, 1977.
9. C.D. McDowell and M.J. Bernstein, "Surface Transfer Impedance of Subminiature Coax Cables," SAMSO-TR-72-276, Aug. 31, 1972.
10. "Test Report, P78-2 Space Vehicle EORC Test," TR5859003, Sept. 29, 1978.

*Blank*

## DISTRIBUTION LIST

### DEPARTMENT OF DEFENSE

Assistant to the Secretary of Defense  
Atomic Energy  
ATTN: Executive Assistant

Defense Intelligence Agency  
ATTN: DB-4C

Defense Nuclear Agency  
2 cy ATTN: RAEV  
4 cy ATTN: TITL

Defense Technical Information Center  
12 cy ATTN: DD

Field Command  
Defense Nuclear Agency  
ATTN: FCLMC  
ATTN: FCPR

Field Command  
Defense Nuclear Agency  
Livermore Branch  
ATTN: FCPRL

Interservice Nuclear Weapons School  
ATTN: TTV

Joint Chiefs of Staff  
ATTN: J-5 Nuclear Division  
ATTN: C3S Evaluation Office

Joint Strat Tgt Planning Staff  
ATTN: JLA  
ATTN: JLTW-2

National Communications System  
Office of the Manager  
Department of Defense  
ATTN: NCS-TS

Undersecretary of Def for Rsch & Engrg  
ATTN: Strategic & Space Systems (OS)  
ATTN: AE

### DEPARTMENT OF THE ARMY

BMD Advanced Technology Center  
Department of the Army  
ATTN: ATC-0

BMD Systems Command  
Department of the Army  
ATTN: BDMSC-H

Deputy Chief of Staff for Rsch Dev & Acq  
Department of the Army  
ATTN: DAMA-CSS-N

Electronics Tech & Devices Lab  
U.S. Army Electronics R&D Command  
ATTN: DRSEL

U.S. Army Communications Sys Agency  
ATTN: ECM-AD-LB

### DEPARTMENT OF THE ARMY (Continued)

Harry Diamond Laboratories  
Department of the Army  
ATTN: DELHD-N-RBC, R. Gilbert  
ATTN: DELHD-I-TL

U.S. Army Foreign Science & Tech Ctr  
ATTN: DRXST-IS-1

U.S. Army Missile R&D Command  
ATTN: RSIC

### DEPARTMENT OF THE NAVY

Naval Research Laboratory  
ATTN: Code 6707, K. Whitney  
ATTN: Code 7550, J. Davis  
ATTN: Code 6701

Naval Surface Weapons Center  
ATTN: Code F31

Strategic Systems Project Office  
Department of the Navy  
ATTN: NSP

### DEPARTMENT OF THE AIR FORCE

Air Force Geophysics Laboratory  
ATTN: PH, C. Pike

Air Force Weapons Laboratory  
Air Force Systems Command  
ATTN: SUL  
ATTN: NT  
ATTN: NXS  
2 cy ATTN: DYC

Ballistic Missile Office  
Air Force Systems Command  
ATTN: MNNH  
ATTN: MNRTE  
ATTN: MNRG

Deputy Chief of Staff  
Research, Development, & Acq  
Department of the Air Force  
ATTN: AFRDQI

Headquarters Space Division  
Air Force Systems Command  
ATTN: SKF

Rome Air Development Center  
Air Force Systems Command  
ATTN: ESR, E. Burke

Strategic Air Command  
Department of the Air Force  
ATTN: NRI-STINFO Library  
ATTN: XPFS

OTHER GOVERNMENT AGENCIES

Central Intelligence Agency  
ATTN: OSWR/STD/MTB, A. Padgett

NASA  
Lewis Research Center  
ATTN: N. Stevens  
ATTN: C. Purvis  
ATTN: Library

DEPARTMENT OF ENERGY CONTRACTORS

Lawrence Livermore National Lab  
ATTN: Tech Info Dept Library

Los Alamos National Scientific Lab  
ATTN: MS 364

Sandia National Laboratories  
Livermore National Laboratory  
ATTN: T. Dellin

Sandia National Lab  
ATTN: 3141

DEPARTMENT OF DEFENSE CONTRACTORS

Aerospace Corp  
ATTN: Library  
ATTN: V. Josephson

AVCO Research & Systems Group  
ATTN: Library AB30

Boeing Co  
ATTN: P. Geren

Computer Sciences Corp  
ATTN: A. Schiff

Dikewood Corporation  
ATTN: Tech Library

Dikewood Corporation  
ATTN: K. Lee

ET&G Washington Analytical Services Ctr, Inc  
ATTN: Library

Ford Aerospace & Communications Corp  
ATTN: A. Lewis  
ATTN: Tech Library

General Electric Co  
ATTN: J. Peden

General Electric Company—TEMPO  
ATTN: W. McNamara  
ATTN: DASAC

Hughes Aircraft Co  
ATTN: Tech Library

Hughes Aircraft Co  
ATTN: E. Smith  
ATTN: W. Scott  
ATTN: A. Narevsky

DEPARTMENT OF DEFENSE CONTRACTORS (Continued)

IRT Corp  
ATTN: B. Williams  
ATTN: Library  
ATTN: N. Rudie  
ATTN: R. Keyser  
ATTN: R. Leaden  
ATTN: S. Weiman  
ATTN: I. Wilk

JAYCOR  
ATTN: E. Wenaas  
ATTN: Library

JAYCOR  
ATTN: R. Sullivan

Johns Hopkins University  
ATTN: P. Partridge

Kaman Sciences Corp  
ATTN: W. Rich  
ATTN: Library  
ATTN: N. Beauchamp  
ATTN: D. Osborn

Lockheed Missiles & Space Co, Inc  
ATTN: Dept 85-85

McDonnell Douglas Corp  
ATTN: S. Schneider

Mission Research Corp  
ATTN: C. Longmire  
ATTN: R. Stettner

Mission Research Corp  
ATTN: B. Goplen

Mission Research Corp-San Diego  
ATTN: V. Van Lint  
ATTN: Library

Pacific-Sierra Research Corp  
ATTN: L. Schlessinger  
ATTN: H. Brode

R & D Associates  
ATTN: S. Siegel  
ATTN: R. Schaefer  
ATTN: Tech Info Center  
ATTN: P. Haas

Rockwell International Corp  
ATTN: Library

Science Applications, Inc  
ATTN: W. Chadsey

Spire Corp  
ATTN: R. Little

SRI International  
ATTN: Library

Institute for Defense Analyses  
ATTN: Classified Library

DEPARTMENT OF DEFENSE CONTRACTORS (Continued)

Systems, Science & Software, Inc  
ATTN: A. Wilson  
ATTN: Library

DEPARTMENT OF DEFENSE CONTRACTORS

TRW Defense & Space Sys Group  
ATTN: D. Clement  
ATTN: Technical Information Center

*Robert*

